Muhammet Furkan Bilgi

DESIGN AND CONTROL OF UNIVERSAL TEST PLATFORM FOR LOWER LIMB ASSISTIVE DEVICES

AGU 2018

DESIGN AND CONTROL OF UNIVERSAL TEST PLATFORM FOR LOWER LIMB ASSISTIVE DEVICES

A THESIS
SUBMITTED TO THE DEPARTMENT OF ADVANCED MATERIALS AND NANOTECHNOLOGY
AND THE GRADUATE SCHOOL OF ENGINEERING AND SCIENCE OF ABDULLAH GUL UNIVERSITY
IN PARTIAL FULFILLMENT OF THE REQUIREMENTS
FOR THE DEGREE OF
M. Sc.

By
Muhammet Furkan Bilgi
December 2018

DESIGN AND CONTROL OF UNIVERSAL TEST PLATFORM FOR LOWER LIMB ASSISTIVE DEVICES

A THESIS

SUBMITTED TO THE DEPARTMENT OF ADVANCED MATERIALS AND NANOTECHNOLOGY

AND THE GRADUATE SCHOOL OF ENGINEERING AND SCIENCE OF ABDULLAH GUL UNIVERSITY

IN PARTIAL FULFILLMENT OF THE REQUIREMENTS

FOR THE DEGREE OF

M. Sc.

By

Muhammet Furkan Bilgi

December 2018

SCIENTIFIC ETHICS COMPLIANCE

I hereby declare that all information in this document has been obtained in accordance with academic rules and ethical conduct. I also declare that, as required by these rules and conduct, I have fully cited and referenced all materials and results that are not original to this work.

Muhammet Furkan Bilgi

REGULATORY COMPLIANCE

M.Sc. thesis titled **"DESIGN AND CONTROL OF UNIVERSAL TEST PLATFORM FOR LOWER LIMB ASSISTIVE DEVICES"** has been prepared in accordance with the Thesis Writing Guidelines of the Abdullah Gül University, Graduate School of Engineering & Science.

Prepared By	Advisor
Muhammet Furkan BİLGİ	Assistant Prof. Ramazan ÜNAL

Head of the Advanced Materials and Nanotechnology Program

Prof. Dr. Murat DURANDURDU

ACCEPTANCE AND APPROVAL

M. Sc. thesis titled "**DESIGN AND CONTROL OF UNIVERSAL TEST PLATFORM FOR LOWER LIMB ASSISTIVE DEVICES**" and prepared by Muhammet Furkan Bilgi has been accepted by the jury in the Advanced Materials and Nanotechnology Graduate Program at Abdullah Gul University, Graduate School of Engineering & Science.

20 /12 / 2018

JURY:

Assistant Professor Ramazan ÜNAL : ……

Associated Professor Günyaz ABLAY : ……..

Associated Professor Recep EKİCİ : ……

APPROVAL:

The acceptance of this M. Sc. thesis has been approved by the decision of the Abdullah Gül University, Graduate School of Engineering & Science, Executive Board dated ….. /….. / …….. and numbered ……..……. .

…….. /…….. / ……..

Graduate School Dean

Prof. Dr. İrfan ALAN

ABSTRACT

DESIGN AND CONTROL OF UNIVERSAL TEST PLATFORM FOR LOWER LIMB ASSISTIVE DEVICES

Muhammet Furkan Bilgi

M.Sc. in Advanced Materials and Nanotechnology Department

Advisor: Assistant Prof. Ramazan ÜNAL

December-2018

Robotic lower limb assistive devices are highly important tools because they are being used in rehabilitation of patients who has problems with their lower limbs or enhancing the capabilty of human such as lifting or carrying high loads. Besides, testing and evaluation of these devices accurately has vital importance. Robotic testing has many advantegeous aspects such as being able to perfom long term operations and mimic dangerous conditions such as near-fall etc. Also, collecting data from test device is easier than collecting from human. First, a conceptual exoskeleton which can perform walking (weight acceptance, push-off and swing), sit to stand and stair climbing tasks is designed. To be able to perform these tasks, springs, an actuator and engage disengage mechanism are mounted on the exoskeleton and coefficient of springs, and required power of actuator are calculated. Secondly, a test platform design is proposed. After that, a controller that is meant to mimic the hip motion (center of mass motion and hip joint) is introduced by using MATLAB-Simulink.

Keywords: Exoskeleton, test platform, test bed, walking, sit to stance, stair ascent.

ÖZET

ALT EKSTREMİTELERE YARDIMCI CİHAZLAR İÇİN ÜNİVERSAL BİR TEST PLATFORMU DİZAYN VE KONTROLÜ

Alt ekstremitelere yardımcı cihazlar, alt ekstremite problemleri yaşayan hastaların rehabilitasyonlarında, ağır yük kaldırma ya da taşıma işlerinde kullanıldıkları için çok önemlidirler. Ayrıca, bu cihazların doğru bir şekilde test edilmesi de ayrıca bir öneme sahiptir. Robotik test uzun dönem test edebilme, düşme vb. tehlikeli durumları cihazla oluşturabilme gibi avantajları vardır. Ayrıca test cihazlarından veri toplamak gerçek insandan veri toplamaktan daha kolaydır. Bu çalışmada ilk olarak yürüme, oturup kalkma ve merdiven çıkma işlerini yapabilecek konsept bir eksoskeleton cihazı tasarlandı. Bu işleri yapabilmesi için eksoskeletona yaylar, motor ve aktif-deaktif mekanizması eklendi ve ardından yay sabitleri, gereken motor gücü hesaplandı. Ardından bir test cihazı tasarlandı ve kalça hareketinin (kütle merkezi hareketi ve kalça eklemi) taklit edilebilmesi için MATLAB- Simulink yardımıyla bir kontrolcü tasarlandı.

Anahtar Kelimeler: Eksoskeleton, test platformu, yürüme, oturup kalkma, merdiven çıkma.

Acknowledgements

I would like to thank my advisor Assistant Prof. Ramazan ÜNAL for his goodwill and help in my study.

I must express my very profound gratitude to my parents and to my wife for providing me with unfailing support and continuous encouragement throughout my years of study and through the process of researching and writing this thesis. This accomplishment would not have been possible without them.

TABLE OF CONTENTS

1. INTRODUCTION 1

2. METHODS 6

2.1 ANATOMICAL TERMS 6

2.2 TERMS OF GAIT 10

2.3 MUSCLES 11

2.3.1 *Task of Lower Limb Muscles 11*

2.4 ANALYSIS 13

2.4.1 Gait Analysis 13

2.4.2 Stair Ascend Analysis 14

3. DESIGN 17

3.1 EXOSKELETON DESIGN 17

3.1.1. Weight Acceptance Spring 18

3.1.2. Sit to Stance Spring 19

3.1.3. Stair Ascent Spring 21

3.1.4. Swing and Push-Off Springs 23

3.1.5. Weight Acceptance Mechanism 26

3.1.6. Results and Discussion of Exoskeleton 29

3.2. TEST BED DESIGN 32

3.2.1. Center of Mass (CoM) Analysis 32

3.2.2. Hip Data Analysis 34

3.2.3. Design 36

4. CONTROL 39

4.1 CONTROL OF CENTER OF MASS (COM) 39

4.2 CONTROL OF THE THIGH 50

5. CONCLUSIONS AND FUTURE PROSPECTS 57

5.1 CONCLUSIONS 57

5.2 FUTURE PROSPECTS 58

BIBLIOGRAPHY 60

APPENDIX 64

List of Figures

Figure 2.1.1 Planes of Body [21] 7
Figure 2.1.2 Movements of a)Hip Joint [22] b)Knee Joint [23] 8
Figure 2.1.3 Motions of Ankle Joint [24] 8
Figure 2.1.4 Angles of Lower Limbs [26] 9
Figure 2.2.1 Gait Cycle [27] 10
Figure 2.3.1.1 Muscles of Lower Limb a) Gluteus Medius[29], b) Gluteus Maximus[29], c) Medial and Lateral Hamstrings[30], d) Erector Spinae[31], e)Sartorius[29], f) Rectus Femoris[29], g) Vastus Lateralis[29], h) Adductor Longus[29], i) Adductor Magnus[29], j) Tibialis Anterior[29], k) Extensor Digitorum Longus[29], l) Medial (Blue) and Lateral (Red) Gastrocnemius[32], m) Soleus[29], n) Peroneus Longus[33] 12
Figure 2.4.1.1 Angle, Moment and Power Graphs of Ankle and Knee Joints During Normal Gait [26] 14
Figure 2.4.2.1 Angle of knee joint during stair ascend [34] 15
Figure 2.4.2.2 Moment of knee joint during stair ascend [34] 16
Figure 2.4.2.3 Power of knee joint during stair ascend [34] 16
Figure 3.1.1 Dimensions used for kinematic calculations 17
Figure 3.1.1.1 Spring of Weight Acceptance 18
Figure 3.1.1.2 Force-Elongation Graph 19
Figure 3.1.1.3 Knee and Spring Torque during WA 19
Figure 3.1.2.1 Sitting Position of Exoskeleton 20
Figure 3.1.2.2 Force-Elongation Graph of Sit to Stance Spring 21
Figure 3.1.2.3 Torque Behaviours of Knee and Spring During Sit to Stance 21
Figure 3.1.3.1 Stair Ascent Actuator 22
Figure 3.1.3.2 Torque comparison between biological knee joint [2] and exoskeleton during stair ascent 22
Figure 3.1.4.1 Pulley and rack-pinion mechanism 23
Figure 3.1.4.2 Elongation vs. force graph for swing spring 24
Figure 3.1.4.3 Moment comparison of actual knee and spring during swing 24
Figure 3.1.4.4 Push-off and swing springs 25
Figure 3.1.4.5 Identifying elastic constant of push-off spring from natural ankle data 26
Figure 3.1.5.1 A simple weight acceptance mechanism 27
Figure 3.1.5.2 The on (a) and off (b) positions 28
Figure 3.1.5.3 Initial (a) and engaged (b) positions 28
Figure 3.1.6.1 Comparison of natural knee joint and exoskeleton a) torque and b) power during WA 29
Figure 3.1.6.2 Comparisonof the knee joint and exoskeleton torque during sit to stand 30
Figure 3.1.6.3 a) Moment and b) Power plots of knee during ascending 31

Figure 3.1.6.4 3D CAD model of exoskeleton design 32
Figure 3.2.1.1 Cam Profile a) Technical Drawing of Cam, b) 3D Model of Cam 33
Figure 3.2.1.2 CoM Motion With Cam 34
Figure 3.2.2.1 Angles of Hip During Normal Walking 35
Figure 3.2.2.2 Hip moment in one single step 35
Figure 3.2.3.1 Concept Designs a) Direct Drive b) Fourbar Mechanism c) Fourbar with Torsion Spring Mechanism 36
Figure 3.2.3.2 Torque Angle Graph of Hip 36
Figure 3.2.3.3 Comparison Graph in terms of a) Angle b) Torque c) Power 37
Figure 3.2.3.4 Concepual design of test bed a) Test bed with cam b) Test bed with ballscrew 38
Figure 4.1.1 Representation of CoM 39
Figure 4.1.2 Simple representation of PID control system 41
Figure 4.1.3 A simple block diagram 41
Figure 4.1.4 Input (a) and output (b) assignments for S-Function Builder 43
Figure 4.1.5 Derivatives section in S-Function Builder 44
Figure 4.1.6 Outputs section of S-Function Builder 45
Figure 4.1.7 Simulink model of the CoM system 46
Figure 4.1.8 Sine wave generator 46
Figure 4.1.9 PID parameters 47
Figure 4.1.10 Result of the simulation 47
Figure 4.1.11 Required force, torque and power for the actuator 49
Figure 4.2.1 CoM and fourbar for thigh actuation 50
Figure 4.2.2 Simulink model of the thigh 52
Figure 4.2.3 PD controller parameters for thigh system 52
Figure 4.2.4 The result of the simulation 53
Figure 4.2.5 Overshoot of the model 53
Figure 4.2.6 Comparison of different derivative gains (a)1.7, b)10, c)20) 55
Figure 4.2.7 Final result of the thigh simulation 56
Figure 5.2.1 Parts of conceptual designs 59

List of Tables

Table 2.1.1 Range of motions of hip, knee and ankle joints [22],[23],[24],[25] 9
Table 2.2.1 Angles and motions of lower limb joints during gait cycle [28] 11

This thesis is dedicated to my family and my wife

Chapter 1

Introduction

The lower limb assistive devices (exoskeletons or prostheses) have become a vital tool employed to assist or augment the capabilities of people in daily activities. First of all, these devices aid amputees, people with muscle weaknesses, gait disorders to walk or perform activities of daily life. Secondly, lower limb assistive devices augment ability to lift and carry heavy loads of people such as infantry soldiers, firefighters, disaster relief workers etc. Another usage of these devices is rehabilitation. These devices are used in order to drive the leg of patients (stroke patient, patients with muscle weaknesses etc.) to track the desired trajectory so that they can re-gain their motor control ability. The design and control of such a system is still in the research phase, and the robotic solution proposal, which can effectively perform the tasks mentioned above has great importance. In recent years, the dynamic modelling of the human body, electro-mechanical and metabolic energy efficiency, and the robust, effective and safe human-robot interaction have attracted considerable attention in the development of assistive devices.

Assistive devices can be classified into three main categories according to their actuation principle: active, passive and semi-active devices. Active assistive devices inject energy to augment humans' or patients' capability by means of using energy sources, actuators and controllers. For example BLEEX is an active device that consists 7 degrees of freedom (DoF) and four of them are actuated by linear hydraulic actuators. It consumes 1140 W of electric power [1]. ALEX is another active assistive device consisting 7 DoF, 2 of which are actuated by linear actuators [2]. There are also some commercial active exoskeletons which are Indego [3], REX [4], ReWalk [5] etc. Passive devices do this task by not injecting external energy but by means of springs, dampers or artificial tendons etc. Exoskeleton that is built in [6] has artificial tendons to build up torques about joints. Exoskeleton in [7] is a passive exoskeleton that has springs to generate torque. FORTIS [8] and Againer [9] can be given as examples for commercial passive exoskeletons. In semi-active devices, actuation is not used to drive the joints

directly but employed to engage or disangage the equipments that generate torque about joints such as springs, dampers, tendons etc. For example in [10], researchers used controlled electromechanical clutch to engage and disangage the spring in order to build up torque about the joint at correct phase of gait. In [11], exoskeleton consists a motorized mechanism to activate and deactivate the spring.

Until today, many research studies on the design of assistive devices either for rehabilitation of patients with gait disorder or augmentation of capabilities of healthy people have been conducted by researchers. Kooij et. al. presented the design and control of LOPES exoskeleton which is designed to train the post-stroke patients [12]. LOPES has impedance control system to establish safe environment for both patients and the therapist. This exoskeleton is mounted to the fixed world at the patient's pelvis height so that the weight of exoskeleton can be carried by the robot's fixed torso. Besides, it allows LOPES to apply torques to pelvis of the patient. In [13], aiding stroke patients who have lack of motor function and decreasing the burden on the clinical staff is aimed by Wu et. al. The exoskeleton has 3 DOFs (Hip, knee and ankle joints in sagittal plane) and 3 actuators at these joints. To be able to control the exoskeleton, researchers implemented adaptive robust sub-controller and PI sub-controller to the system. Kinematic model of exoskeleton, motor model and friction model were derived. Friction model was taken into account to achieve better results by adding friction torque into mathematical model. In addition to this, exoskeleton consists of safety measures. For this, 2 emergency stops are mounted on the exoskeleton so that patients can stop the system when they feel any discomfort during training.

An ankle foot orthosis consisting of myoelectric controller is described by Ferris et. al. [14]. This ankle-foot orthosis also has two pneumatic muscles of which one of them provides plantarflexion motion and the other one drives the ankle to perform the dorsiflexion motion. The reason lying behind using the pneumatic muscles is that they can provide high amount of torques with relatively low weight. The ankle-foot orthosis in previous work, [15], showed efficient performance to supply high torques around the ankle yet caused difficulty to the patient for donning and doffing. In order to overcome this problem, researchers used a bivalve carbon fiber construction with plastic buckles. Besides, to be able to provide air supply to pneumatic muscles, EMG signals were used. Experiments that is performed with a subject (age 30 years and weighs 91 kg) showed that the subject can travel immediately with the device when the myoelectric controller

was turned on. In [2], Banala et. al. presented Active Leg Exoskeleton (ALEX) which is designed for rehabilitation of patients who have walking disabilities. In ALEX, researchers used force field controller to drive the leg to move in the desired trajectory. The paradigm behind this controller is assist-as-needed. The main idea of this paradigm is applying force if movement of the leg deviates from the desired trajectory. Assist-as-needed would be a better approach because experiments carried out by Cai et. al. revealed that forcing patient to follow predetermined trajectory may causes learned helplessness [16]. Yet, assist as needed needs backdrivable actuator because this method interacts with the user and controls the device according to data which is applied by the patient to exoskeleton. Also, Banala et. al. proposed two control methods: model based compensation and load cell based compensation. In ALEX, load cell based compensation was used. ALEX showed %60 reduction on patient's trajectory deviations.

In [17], Jezernik et. al. designed Lokomat to train the patients with SCI (Spinal Cord Injury) disease and stroke patients. Lokomat has 4 degrees of freedom. These DoFs are actuated by four linear actuators and a parallelogram (provides vertical up and down motion of the patient. Linear actuators are mounted on the Lokomat's upper and lower leg segments. These actuators also have force sensors. Four independent PD position controllers are tracking the reference hip and knee joint angles. Precision potentiometers are used to measure the actual joint angles. In addition to these, three advanced control schemes were aplied to Lokomat to allow patients to participate more into rehabilitation process in order to increase their motivation.

In [11], energetically-autonomous powered knee exoskeleton to assist running was described. This exoskeleton aims reducing metabolic cost during running. It has a mechanism to activate and deactivate the spring in order to store and release the energy during running. Spring parallel to the knee joint is engaged between heel strike and toe off, and disengaged during swing phase. The controller of the exoskeleton that is disengaging and engaging the spring is based on estimating the phase of gait and angle of the knee by means of optical encoder and rotary potentiometer. In Nanyang Technological University, an exoskeleton was designed to assist people such as infantry soldiers, fire fighters etc. to carry and travel with heavy loads such as food, weaponry, rescue equipments etc. To be able to control the gait and keep the exo-human in balance, researchers divided the control algorithm into two sub control methods: Control of the leg trajectory and control of ZMP (Zero Moment Point) which is a point that all the net

forces and torques have no horizontal components. To be able to control the trajectory of the gait, researchers have chosen to control the swinging foot's trajectory. They collect data from sensors of swinging foot and drive the leg of exoskeleton to follow the desired trajectory by means of actuators. Besides, there is also another term called support area. Support area corresponds to the supporting foot's area during single support in gait. It also means the area between foots during double support. It is indicated that if ZMP of exoskeleton can be kept in the support area, the balance of gait can be provided. In order to measure the ZMP, a footpad with four force sensors is built. After finding the position of ZMP, actuators are being driven to keep ZMP of exoskeleton around the desired ZMP [18].

In [1], Berkeley Lower Extremity Exoskeleton (BLEEX) is presented. The main goal of the researchers of BLEEX is to be able to carry and travel with heavy load on even difficult type of terrains. According to Zoss et. al., previous exoskeletons have a major problem of not being independent from a power source. BLEEX has its own power supply. It also comprises a pair of leg, 7DOFs for each leg (3 DOFs at hip and ankle, 1 DOF at knee), linear hydraulic actuators and electronics. The reason of using hydraulic actuators is that they have high power to weight ratio. BLEEX controller was designed so that it replicates the motion of the wearer. Measurements are collected from the exoskeleton only, not from the wearer or the contact points of wearer and exoskeleton. Kazerooni et. al. divided the gait into three parts which are single support phase, double support phase and single support with one redundancy in order to establish the model of gait [19]. Experiments performed with 75 kg subject revealed that BLEEX accomplished its main goal which is walking on any type of terrain and carrying heavy load. While doing this, BLEEX consumes 1140 W power during gait. Shamaei et. al. presented a quasi-passive knee exoskeleton in [10]. This exoskeleton comprises two springs and an electromechanical clutch mechanism for each leg in order to assist the knee to accept and release weight during gait. The philosophy behind assisting weight acceptance is engaging the springs during weight acceptance (during flexion of knee) and releasing the energy during extension of the knee. In conclusion, employing this quasi-passive knee exoskeleton revealed that besides providing more comfort to subject, it can be used to examine the knee joint's behaviour in interaction with external impedances [10].

Assistive lower limb devices are tools that are supposed to carry out important tasks for healthy, patient or handicapped people in daily life. Because of this, testing and

evaluation of these devices quantitatively are very important for determining the performance of the design of an assistive device. In addition exoskeletons and prostheses are devices that must have long working life without failure. There are two types of testing and evaluation types for assistive devices which are conventional (using healthy or patients as subjects) and robotic (using test bed/platform) testing method. In conventional testing, justified device with METC protocol, subjects and at least one observer are required in order to test and validate the device. This type of testing causes some problems. One of the most important problem is safety concerns of subjects. It is unsafe to use individuals during testing because when an emergency situation happens, the subject may get hurt. Besides, it can be highly dangerous to test conditions that is considered as unsafe for patients such as near-fall or loss of balance with subjects. In addition to these, conventional testing is not suitable for tough terrains in terms of safety requirements Another limitation of conventional testing is lack of repeatibility. Assistive devices must have long working life so that they can serve individuals without any failure for a long time. Therefore, these devices necessitate testing with high repetition in order to determine the failure and fatigue time of the device. Using subjects for this aim is not feasible. Besides, it is very hard to collect data from subject because alignment between the device and subject may not be fully provided. Richter et. al. indicated that robotic testing can decrease or completely remove these problems, in fact it can provide advantages. For example, testing robots can be programmed in order to provide conditions which are considered as dangerous such as near-fall condition. Also a robot can carry out long term operations to test mechanical durability of assistive device prototype. In addition to that, robots can consist sensors which makes it easier to collecting data than collecting data from subject [20]. Even though robotic testing has many advantages, testing with subjects is needed to be performed after verification of the device with robotic testing because these devices will be used by subjects ultimately and they are needed to be examined in terms of compliance, alignment with limbs, comfort etc.

In this project, designing a universal test platform that mimics the hip behaviour in walking, sit-to-stance and stair climbing motions for the evaluation of the design, controller of assistive devices. Note that high repetition or simulation of dangerous situations like near-fall conditions are not aimed in the scope of this design study. In addition to this, design and control of lower limb exoskeleton has been presented.

Chapter 2

Methods

In order to design suitable active lower limb assistive device for daily usage, biomechanics of lower limb, lower limb muscles that govern the movement of lower extremities and data of gait, sit to stand and stair ascent-descent movements need to be examined. This is very important step to determine springs, actuators, locking mechanisms etc in the design of an assistive device replicating or actuating the human lower limb to follow a desired trajectory in parallel with the bones and muscles. In this section brief explanation of biomechanics of the lower limb, lower extremity muscles, data of gait, sit to stand and stair ascent-descent movements are explained.

2.1 Anatomical Terms

To be able to understand the movements of lower extremities, human body planes are needed to be explained. There are three planes that are coronal, transverse and sagittal plane. Coronal plane is the plane dividing the body into front and back parts. Transverse plane is the plane splitting the body into upper and lower parts. Lastly, the sagittal plane is the plane dividing the body into left and right parts. These planes are shown in Figure 2.1.1.

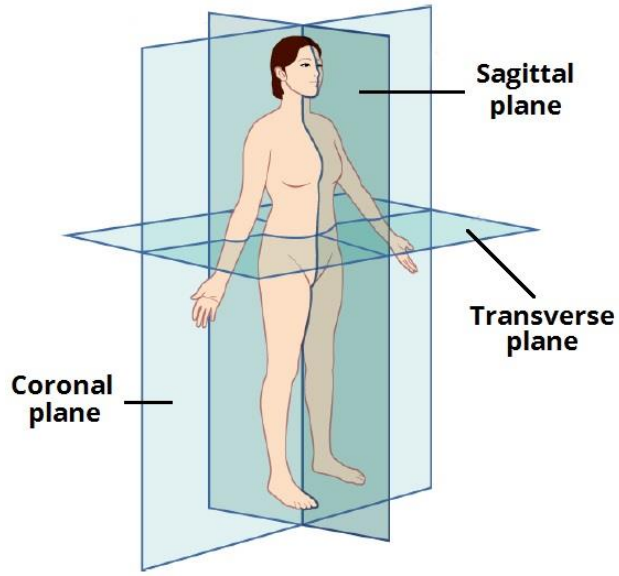

Figure 2.1.1 Planes of Body [21]

Lower extremities make movements in these planes. For the hip joint there are extension, flexion, abduction, adduction and lateral-external rotation. Extension of hip is decreasing of θ_h in sagittal plane, flexion is vice versa. Abduction is increasing of angle between legs in coronal plane while adduction means vice versa. Internal rotation means turning of leg as so toes gets closer to each other while external rotation means the opposite. It is indicated in [22] that the maximum angle hip joint can supply for flexion, extension, abduction, adduction, internal rotation and external rotation are 120°, 10°, 70°, 70°, 50° and 50° respectively. These motions are depicted in Figure 2.1.2-a.

Knee joint can supply extension-flexion, abduction-adduction, internal-external rotation, medial-lateral translation and anterior-posterior translation movements. Flexion of knee means increasing of θ_k in sagittal plane while extension means the opposite of flexion. In [23], Shenoy et. al. suggests that knee joint is able to supply 160° movement. It is also indicated that walking with normal speed, climbing stair, descending stair and making squat exercise need 60°, 80°, 90°, 130° maximum motion range, respectively. Abduction-adduction movements take place in coronal plane. When abduction occurs knee rotates so that knee moves away from the other knee in coronal plane. Adduction means vise versa. Internal rotation of the knee is rotating of knee joint so that toes get closer to each other. External rotation is the opposite of internal rotation movement. Internal and external rotations occur in transverse plane. Medial and lateral translation is linear motion of knee joint in coronal plane. Anterior-posterior translation is moving linearly in sagittal plane. All the motions of knee joint can be seen in Figure 2.1.2-b.

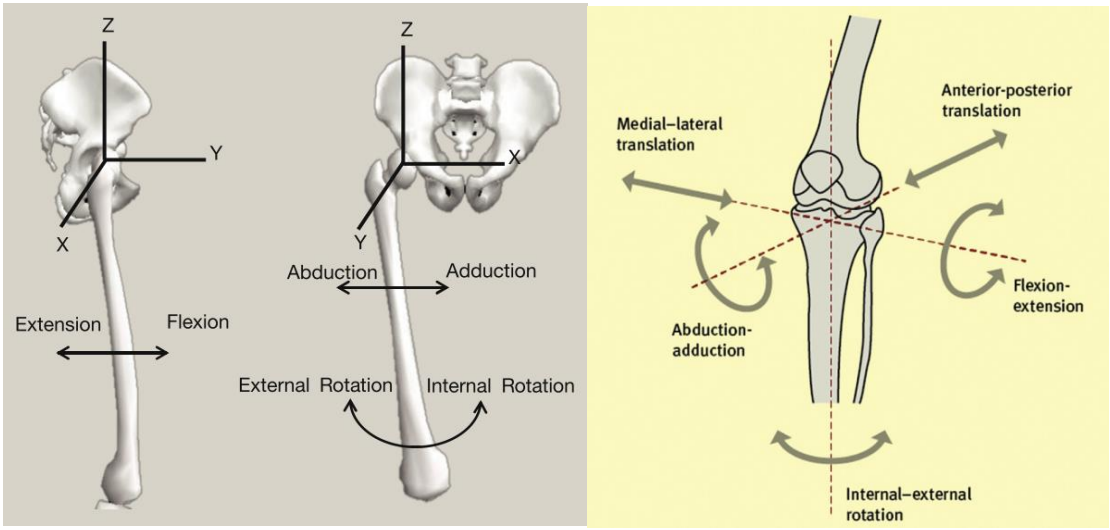

Figure 2.1.2 Movements of a)Hip Joint [22] **b)Knee Joint** [23]

Ankle joint makes dorsiflexion-plantarflexion, inversion-eversion and internal-external axial rotation movements. Dosiflexion is the decreasing the angle of ankle in sagittal plane. Plantarflexion is the opposite of dorsiflexion. Inversion motion is rotation of ankle inward in coronal plane while eversion is rotation motion outward in the same plane. Internal and external rotation motion is rotation inward and outward respectively, in transverse plane. It is indicated in [24], for dorsiflexion motion ankle joint can rotate in the range of 10° to 20° and 40° to 55° for plantarflexion. Besides, ankle joint rotates in 35° range of motion (23° inversion 12° eversion). Motions of ankle joint can be seen in Figure 2.1.3

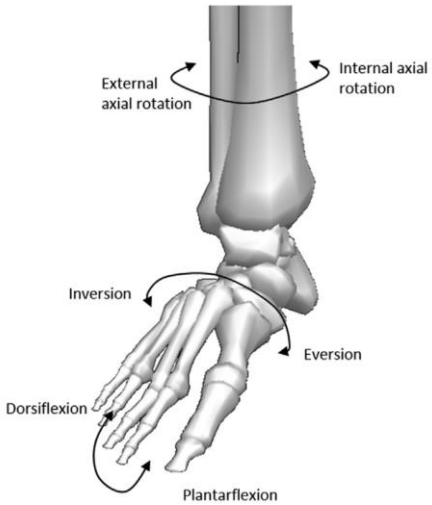

Figure 2.1.3 Motions of Ankle Joint [24]

Motion	Hip	Knee	Ankle
Extension	120°	160°	-
Flexion	10°	3°	-
Abduction	70°	30°	
Adduction	70°	30°	
Internal Rotation	50°	25°	
External Rotation	50°	18°	
Dorsiflexion	-	-	20°
Plantarflexion	-	-	55°
Inversion	-	-	23°
Eversion	-	-	12°

Table 2.1.1 Range of motions of hip, knee and ankle joints [22],[23],[24],[25]

In this thesis, since the main torque generation and power flow occurs and also the motion in abovementioned tasks is dominant in sagittal plane, the movements only in the sagittal plane are examined. It is also important to define the angles of the lower limb in sagittal plane to be able to define the movements of limbs. The angles of limbs in sagittal plane are presented in Figure 2.1.4.

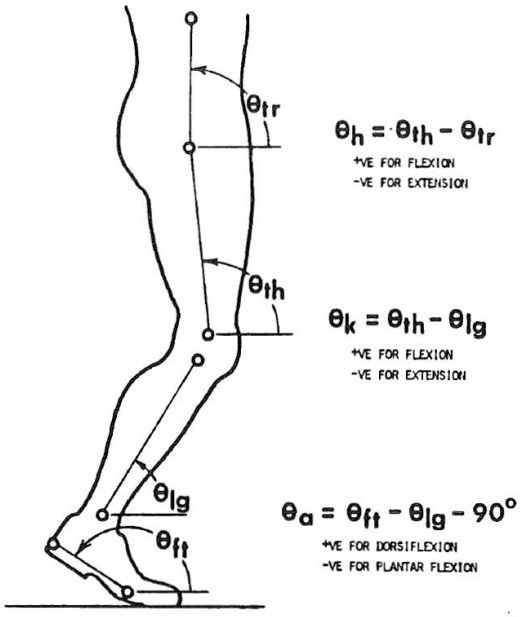

Figure 2.1.4 Angles of Lower Limbs [26]

2.2 Terms of Gait

In order to classify the gait and to be able to communicate on gait in easy way, scientists have been defined some terms. These terms are important to understand the dynamics of gait. These terms are briefly explained in this chapter.

- **Heel Contact (HC):** The moment at which the heel touches the ground.
- **Foot-Flat (FF):** The moment at which the foot become parallel to the ground.
- **Heel-Off (HO):** The first moment at which the heel leaves the ground.
- **Toe-Off (TO):** The first moment at which the toe leaves the ground
- **Stride Period:** The duration of two steps.
- **Step Period:** The duration of one step
- **Double Support:** Part at which two foots touch the ground
- **Single Support:** Part at which one foot touches the ground
- **Stance:** The phase that foot touches the ground
- **Swing:** The phase that the leg rotates freely
- **Weight Acceptance (WA):** The duration between HC and maximum knee flexion during stance phase
- **Push-Off:** The duration at which ankle generates power and push the leg away from ground

These instants and periods are depicted in Figure 2.2.1 gathered from [27].

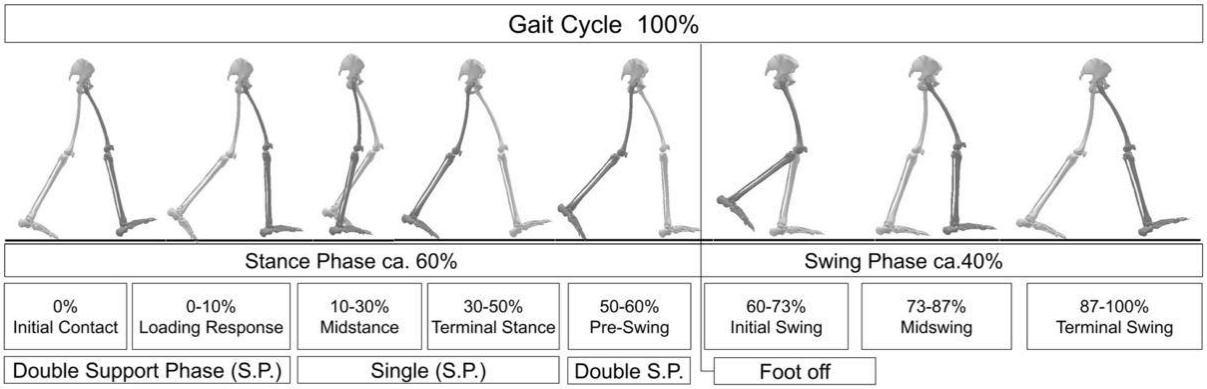

Figure 2.2.1 Gait Cycle [27]

Gait Phases	Initial Contact	Weight Acceptance	Mid Stance	Terminal Stance	Pre Swing	Initial Swing	Mid Swing	Terminal Swing
Gait Cycle	0%	0-10%	10-30%	30-50%	50-60%	60-73%	73-87%	87-100%
Hip	20° flexion	20° flexion	0° flexion	20° extension	10° extension	15° flexion	25° flexion	20° flexion
Knee	0°-5° flexion	20° flexion	0°-5° flexion	0°-5° flexion	40° flexion	60°-70° flexion	25° flexion	0°-5° flexion
Ankle	0°	5°-10° plantarflexion	5° dorsiflexion	10° dorsiflexion	15° plantarflexion	5° plantarflexion	0°	0°

Table 2.2.1 Angles and motions of lower limb joints during gait cycle [28]

2.3 Muscles

There are sixteen muscles that operates in work of lower limbs. These muscles are Gluteus Medius, Gluteus Maximus, Medial and Lateral Hamstrings, Erector Spinae, Sartorius, Rectus Femoris, Vastus Lateralis, Adductor Longus, Adductor Magnus, Tibialis Anterior, Extensor Digitorum Longus, Medial and Lateral Gastrocnemius, Soleus, Peroneus Longus [26]. These muscles are depicted in Figure 2.3.1.1. These muscles have vital role in activities and motions that are done by lower limbs such as walking, sit to stance, ascending-descending stairs and the motions that are described above etc. Even a small flaw in a muscle can make these activities very difficult for human beings. Every muscle have specific tasks and they have to work synchronously with other muscles in order to execute the motions and activities.

2.3.1 Task of Lower Limb Muscles

In this chapter, specific tasks of these muscles are briefly explained. Gluteus Medius muscle has three main objectives. Firstly, it controls the trunk during weight acceptance phase. Secondly, it controls the hip flexion and finally, it operates the swing of limb. Gluteus maximus act as hip extensor. This muscle helps the control of the forward rotation of the body during weight acceptance. It also has a task in swing of limb which is decelerating the limb. Medial hamstrings decelerates the swinging limb and it helps the forward rotation of the thigh. Lateral hamstrings has same task with medial hamstrings. Erector spinae muscle operates the balancing the trunk during weight acceptance phase. Sartorius has functions that are to act as a hip flexor and assisting the swing of lower limb. Rectus femoris muscle act as a knee extensor and hip flexor. Vastus Lateralis assist the knee flexion during weight acceptance phase. Adductor longus muscle serves as a assistive muscle for weight acceptance and thigh accelerating muscle during swing.

Adductor magnus muscle has similar function with the adductor longus muscle. Tibialis anterior keeps the foot in dorsiflexed position and after heel contact it makes the foot flatted to the ground. Extensor digitorum longus muscle has the same function with tibialis anterior muscle. Medial gastrocnemius elongates for the leg to rotate forward between foot flat (5% of stride) to 40% of stride. This muscle also assists the push-off motion. Lateral gastrocnemius musle has exactly the same activity with the medial gastrocnemius muscle. Soleus muscle makes the ankle push-off motion between 40-60% of stride. All these muscles can be seen in Figure 2.3.1.1.

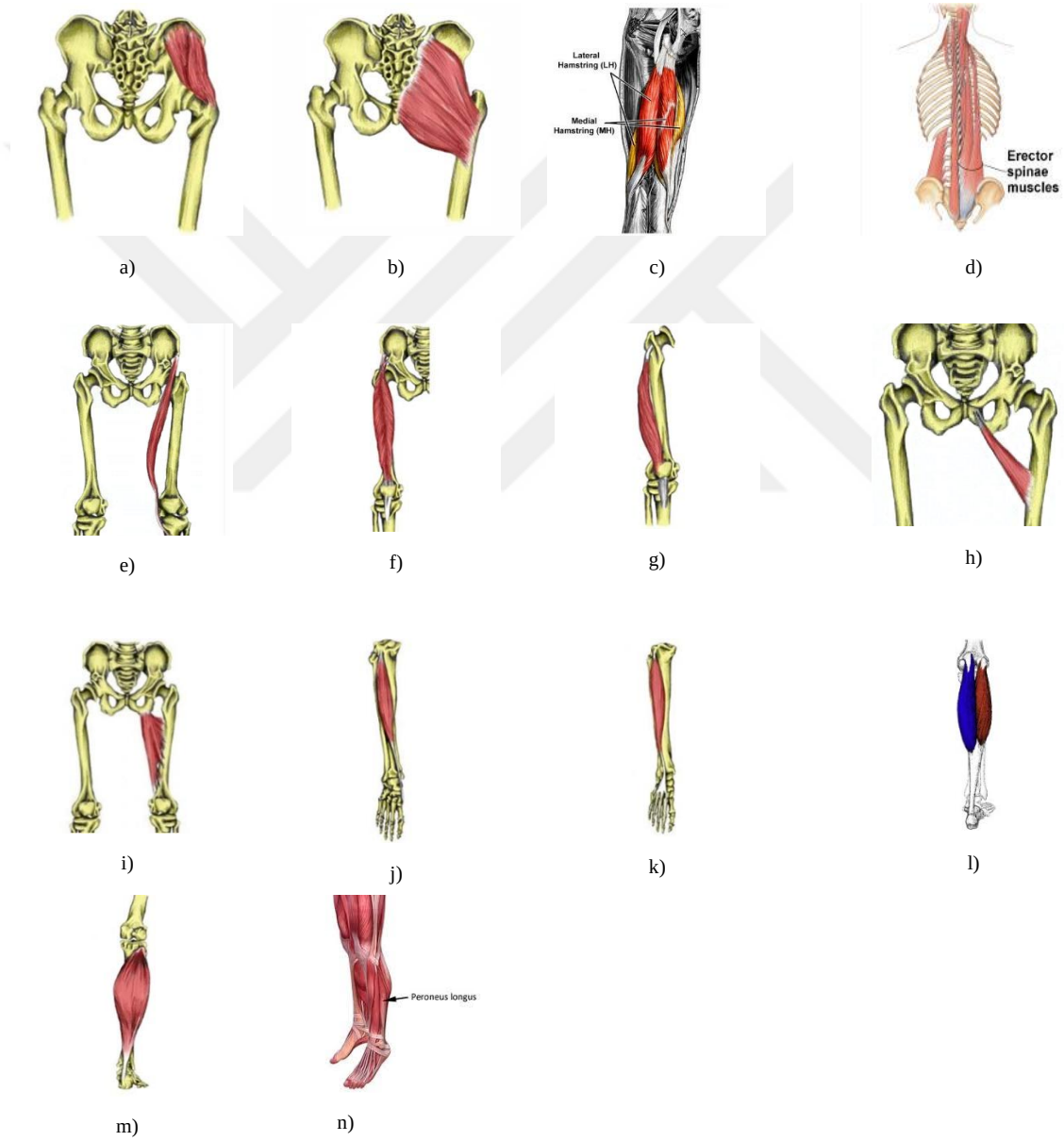

Figure 2.3.1.1 Muscles of Lower Limb a) Gluteus Medius[29], b) Gluteus Maximus[29], c) Medial and Lateral Hamstrings[30], d) Erector Spinae[31], e)Sartorius[29], f) Rectus Femoris[29], g) Vastus Lateralis[29], h) Adductor Longus[29], i) Adductor Magnus[29], j) Tibialis Anterior[29], k) Extensor Digitorum Longus[29], l) Medial (Blue) and Lateral (Red) Gastrocnemius[32], m) Soleus[29], n) Peroneus Longus[33]

2.4 Analysis

2.4.1 Gait Analysis

To be able to understand the dynamics of gait, it is very essential to analyse actual data and graphs. For this purpose, data gathered from [1] is used. In Figure 2.4.1.1, one can see the graph of angle, torque and power of ankle and knee joints. For ankle, there are two terms which are called as dorsiflexion and plantarflexion. Dorsiflexion is decrease in the angle between foot and knee while plantarflexion means increase in the angle between foot and knee. For knee joint, flexion and extension terms exist. Flexion means decrease in angle between knee and shank. Extension means vice versa. Besides, in power graphs, there are areas under and above the zero line. The areas under zero line are part of the gait where joint absorbs energy. Quite the contrary of this, areas above the zero line are part of the gait where joint generates energy.

In the first flexion of the knee in graph (Figure 2.4.1.1), stride between 0-14%, the knee accepts the body weight (weight acceptance) which corresponds to the K1 area in power graph of the knee. K1 is the largest energy absorbtion area in gait. Then the knee extends, stride between 14-40%, to lift the body (Area K2). This first extension after first flexion can be seen as releasing the energy that is stored in the first flexion part of gait by means of muscles around the knee joint. After this, the second flexion occurs (K3). Second flexion plays a vital role during gait. It occurs to prevent foot to strike to the ground. In the 60% of the stride, toe-off (TO) which means the first moment of toe to discontact with the ground occurs. Then the second extension of knee takes place during gait (K4).

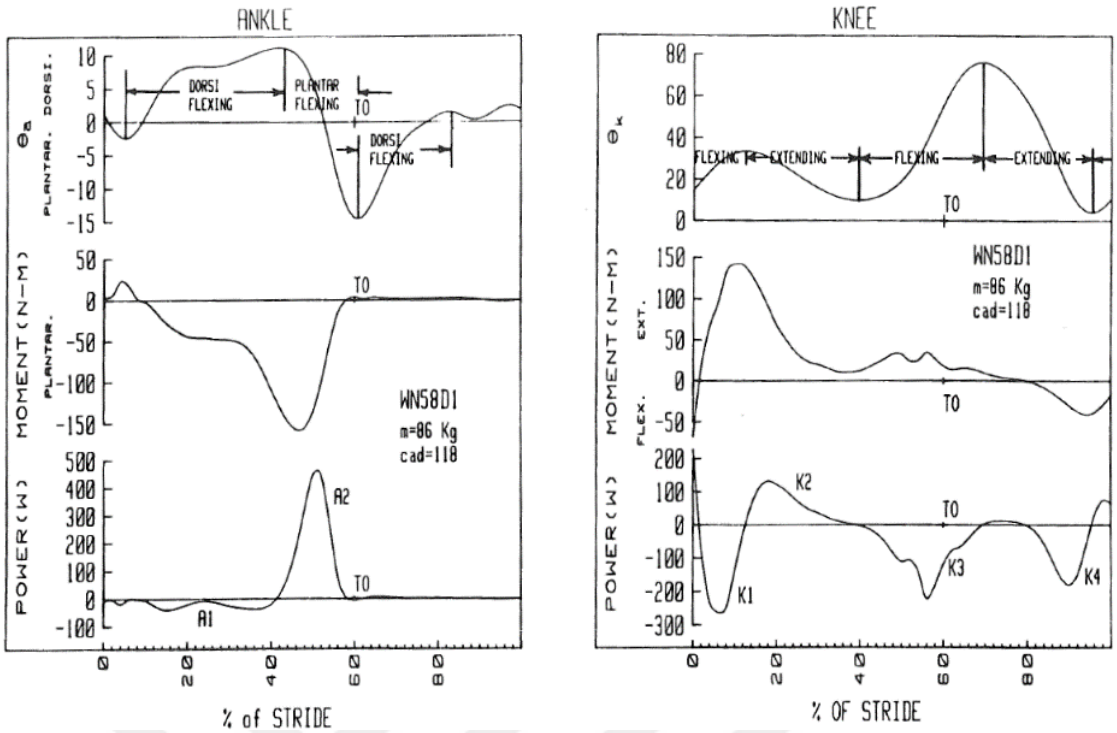

Figure 2.4.1.1 Angle, Moment and Power Graphs of Ankle and Knee Joints During Normal Gait [26]

In the first dorsiflexion of the ankle, the ankle joint stores small amount of energy. After this dorsiflexion, plantarflexion motion occurs. It corresponds to the A2 area which is the biggest energy generation of the ankle joint during gait. This high amount of energy generation is caused by push-off motion of the ankle. Push-off is the part of the gait where ankle plantarflexes and lifts the body around the ball of the foot. This plantarflexion takes place between the 40% and 60% (toe-off moment) of stride. At last, a dorsiflexion occurs. There is very small energy storage (nearly zero) because at this moment, the foot does not touch the ground. This negligible amount of energy mentioned above comes from the ankle making foot to move around the ankle joint in the air.

2.4.2 Stair Ascend Analysis

Stair ascend is the one of the vital tasks that lower limbs perform. This task can be performed by healthy individuals easily but the ones those have handicaps such as stroke, obesity or lack of motor abilities. Since the stair ascend is one of the most important task in daily life, it is highly important to understand this task properly.

Knee joint undertakes the significant part of the stair ascend motion. Figure 2.4.2.1 depicts the angle of knee joint during stair ascend. Riener et. al. started the ascend motion

when one foot is on the next step of the other foot. Knee joint starts its first extension motion with approximately 70° and decreases almost linearly to half of one cycle then it flexes up to nearly 95°. After that, second extension motion takes place until the knee joint reaches to nearly 70°.

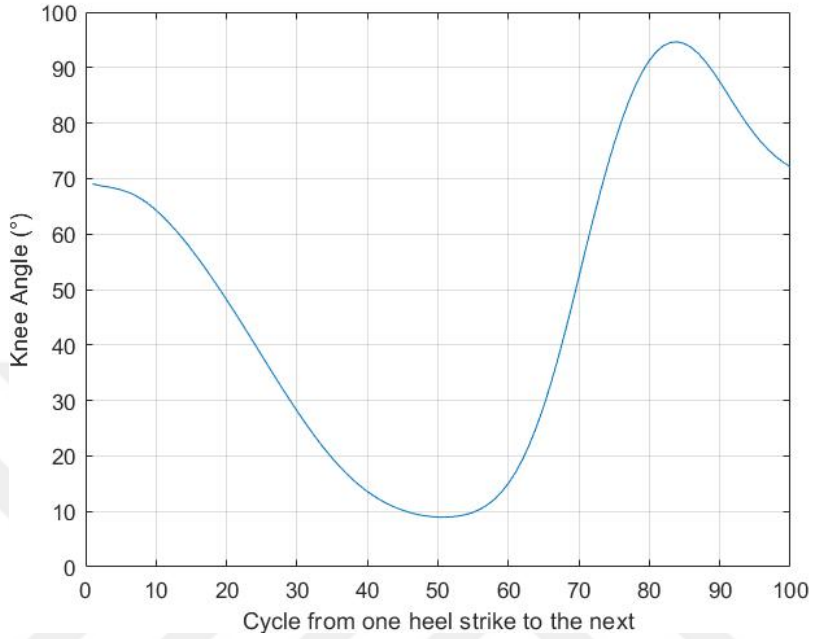

Figure 2.4.2.1 Angle of knee joint during stair ascend [34]

Moment of the knee joint is depicted in Figure 2.4.2.2. Moment starts from nearly zero and increases to 1.1(Nm/kg) until 18% of the cycle is done. Then it decreases to -0.2(Nm/kg) (52%). About 52% of the cycle, the moment reverses in sign. The reason is that the knee joint changes its motion from extension to flexion around that point. Until the end of the cycle, some fluctuations in moment occurs. It is stated in [34] that toe off takes place at 60% of the cycle. Knee joint produces small amount of moment during swing phase, since only the moment that is needed for raising the leg is generated.

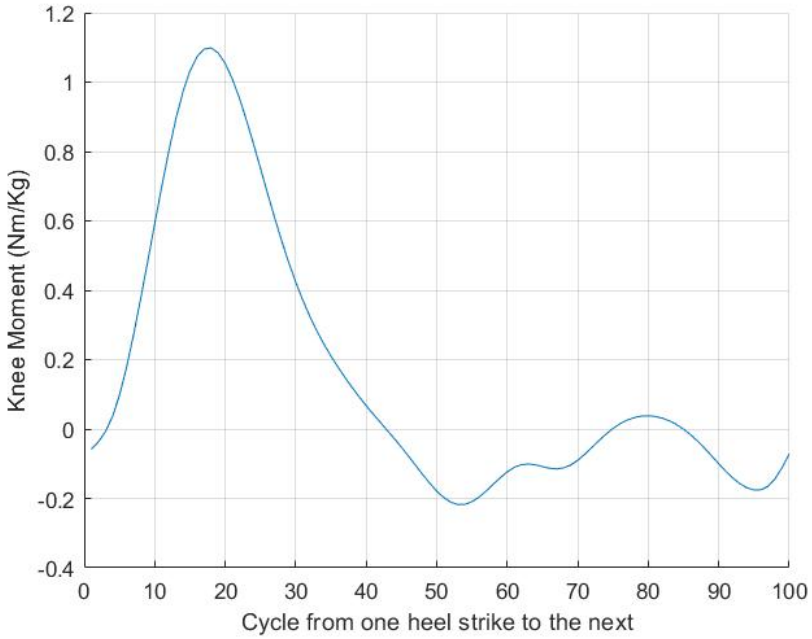

Figure 2.4.2.2 Moment of knee joint during stair ascend [34]

Power graph of knee joint can be seen in Figure 2.4.2.3. Power of the knee joint starts from 0 (W/kg) to 2.5 (W/kg) and decreases to 0 (W/kg) (55%). Then small fluctuations occur as in the moment graph.

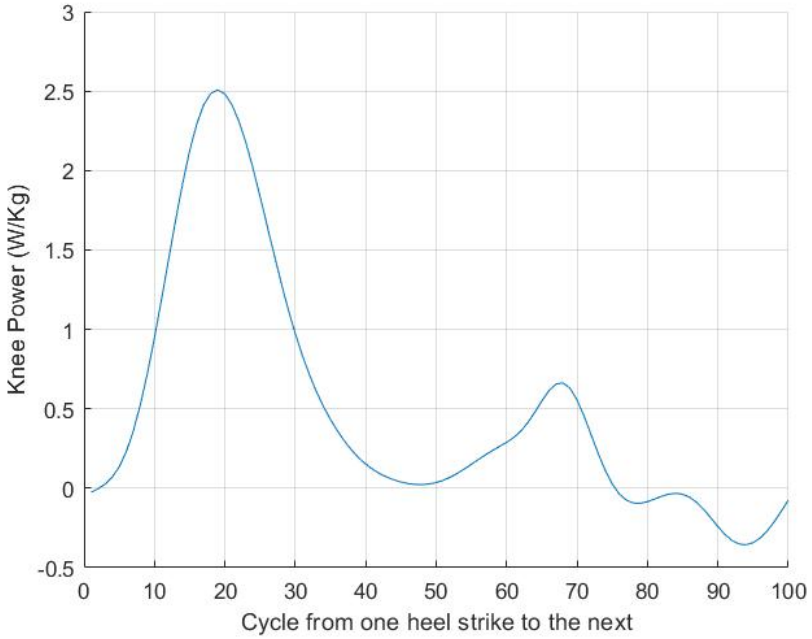

Figure 2.4.2.3 Power of knee joint during stair ascend [34]

Chapter 3

Design

3.1 Exoskeleton Design

In order to build an effective exoskeleton, elastic elements and actuators were used so that the device can replicate the certain tasks of lower limbs such as walking (weight acceptance, push-push-off), sit to stance and stair ascending. To achieve this goal, spring coefficients and the actuator requirements must be determined by using kinematics and dynamics of the device during these tasks. Since the inertias of the links are small and the motion is very slow, they are negligible. So the quasi-static calculations would be sufficient to build an exoskeleton.

First, the kinematic representation of the exoskeleton must be examined. Figure 3.1.1 shows some dimension that were used for kinematic calculations. Matlab codes of the calculations can be seen in the appendix (3.1.1-3.1.4).

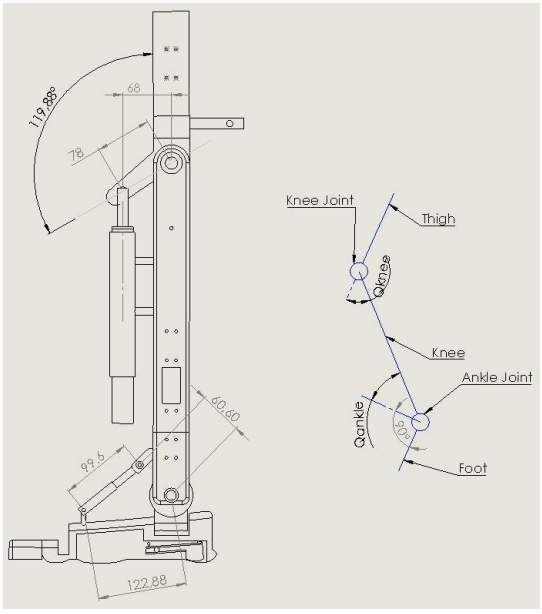

Figure 3.1.1 Dimensions used for kinematic calculations

3.1.1. Weight Acceptance Spring

During walking, the knee joint produces the highest torque in weight acceptance phase of gait. Torque increases and decreases approximately in linear way. It shows that a linear spring can be employed to accept and lift up the weight during gait.

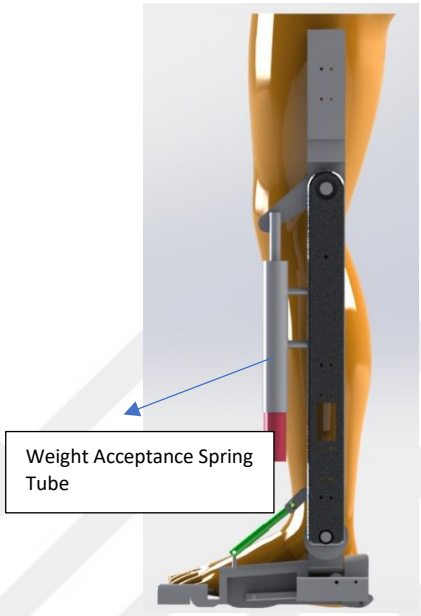

Figure 3.1.1.1 Spring of Weight Acceptance

Two characteristic behaviors can be seen in Figure 3.1.1.2. The behavior with high slope represents the weight acceptance, and the other one represents the push-off and swing phase of gait. It is very important to determine the spring coefficient in order to make the weight acceptance properly. To do this, we must examine the force that is needed to produce knee torque vs. elongation of spring graph. Figure 3.1.1.2 depicts the force-elongation graph for WA spring. In order to determine the spring coefficient, the slope of the red line must be calculated.

$$k_{Weight\ Acceptance} = \frac{167.1 - (-114.8)}{0.01622 - (-0.003208)} = 14500\ [N/m] \quad (3.1.1.1)$$

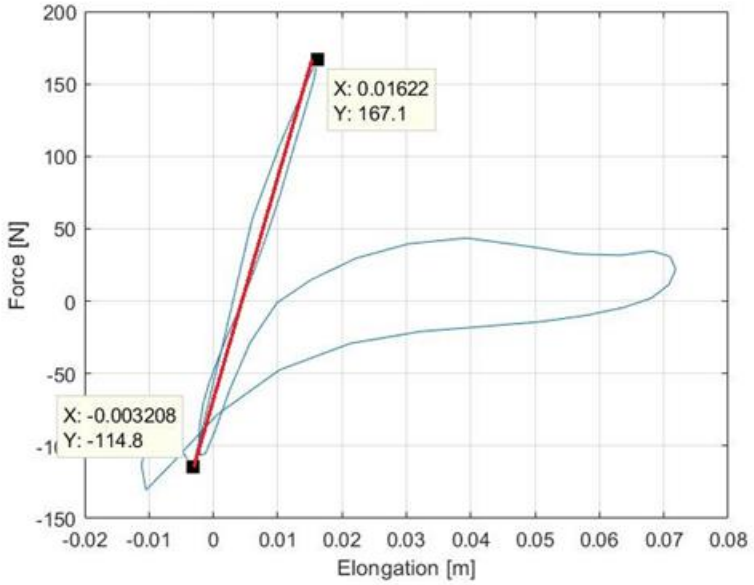

Figure 3.1.1.2 Force-Elongation Graph

After the spring is attached to the system, simulation result shows that our spring behaves like knee joint during WA phase in Figure 3.1.1.3.

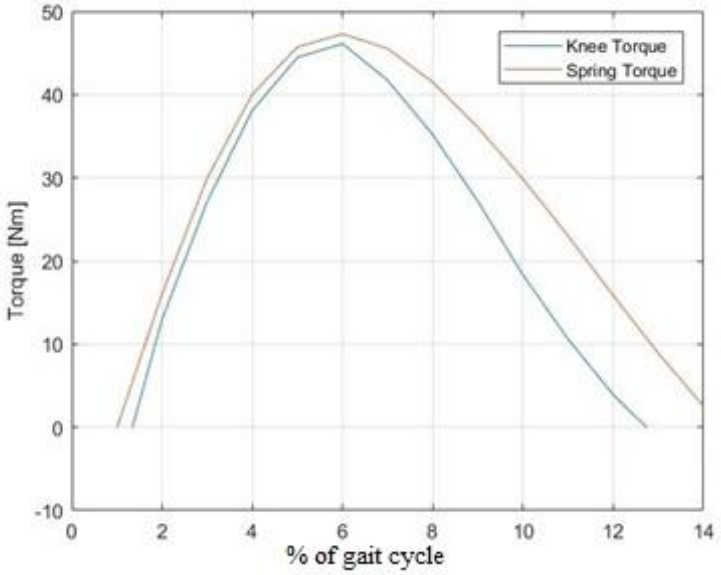

Figure 3.1.1.3 Knee and Spring Torque during WA

3.1.2. Sit to Stance Spring

In order to analyse the sit to stance motion, the torque that is needed for sit to stance motion is calculated quasi-statically because the motion is relatively slow and

inertia effects can be neglected. Sitting motion of the exoskeleton is shown in Figure 3.1.2.1. We assigned the rest of the upper body mass as 50 kg.

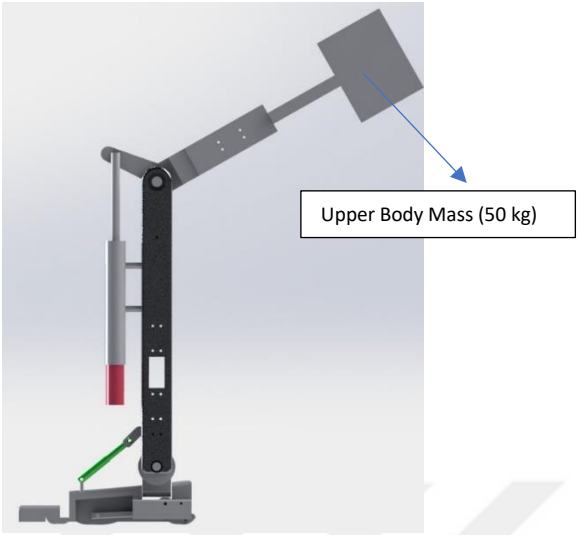

Figure 3.1.2.1 Sitting Position of Exoskeleton

To be able to find the spring coefficient, force that is needed to produce knee torque vs. elongation of spring graph must be analyzed. Figure 3.1.2.2 depicts the force vs. elongation graph of the sit to stance spring. The slope of the red line gives the spring coefficient which is:

$$k_{Sit\ to\ Stance} = \frac{2152 - 489.6}{0.1488 - 0.04103} = 15425\ [N/m] \qquad (3.1.2.1)$$

Because of the $k_{Sit\ to\ Stance}$ value is very close to the $k_{Weight\ Acceptance}$, it seems appropriate to use same spring for both weight acceptance and sit to stance tasks. Besides, behaviour of the spring torque for the sit to stance is approximately same as the knee torque behaviour which can be seen in the graph in Figure 3.1.2.3. There is some difference between the biological knee and exoskeleton torque. This is due to linearization of the force-elongation curve.

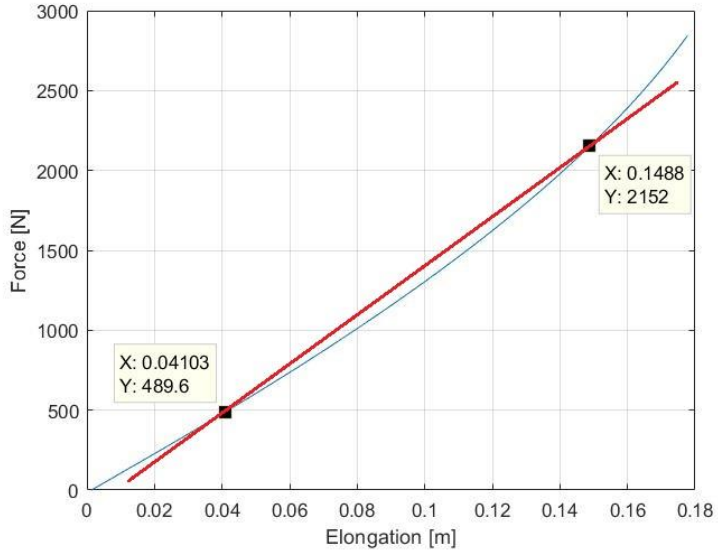

Figure 3.1.2.2 Force-Elongation Graph of Sit to Stance Spring

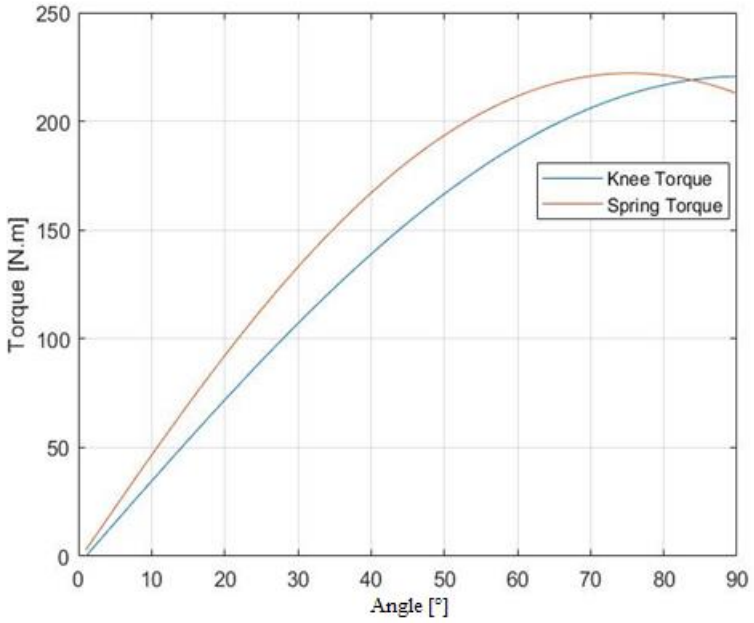

Figure 3.1.2.3 Torque Behaviours of Knee and Spring During Sit to Stance

3.1.3. Stair Ascent Spring

The third goal of our exoskeleton is to assist the stair ascent motion. For assisting to stair ascending we used an actuator including a dc motor with spring mechanism to mimic the knee joint. After analyzing the stair ascending data, the spring that is employed on the actuator to reduce the motor size for generating the stair ascent motion is determined.

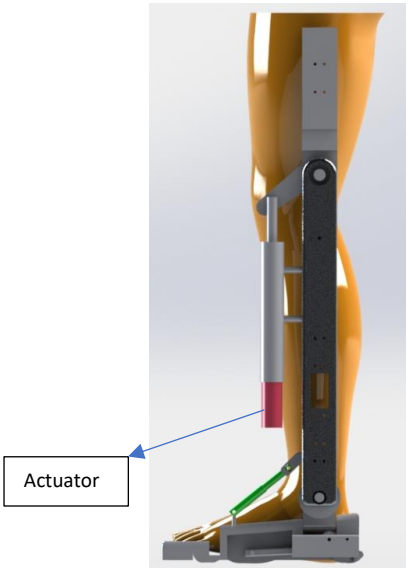

Figure 3.1.3.1 Stair Ascent Actuator

For this purpose, weight acceptance spring is used accompanied by a dc motor with ballscrew transmission. When the simulation of this spring is carried out for the stair ascent motion, the plot in Figure 3.1.3.2 is obtained. At the beginning of stair ascent motion, required torque is nearly 0 Nm but the spring's torque is at nearly 80 Nm. Therefore the spring must be loaded by an actuator to accomplish the lifting up the body weight motion during stair ascent. After loading the spring, actuator starts to release the spring so the spring can produce the desired torque.

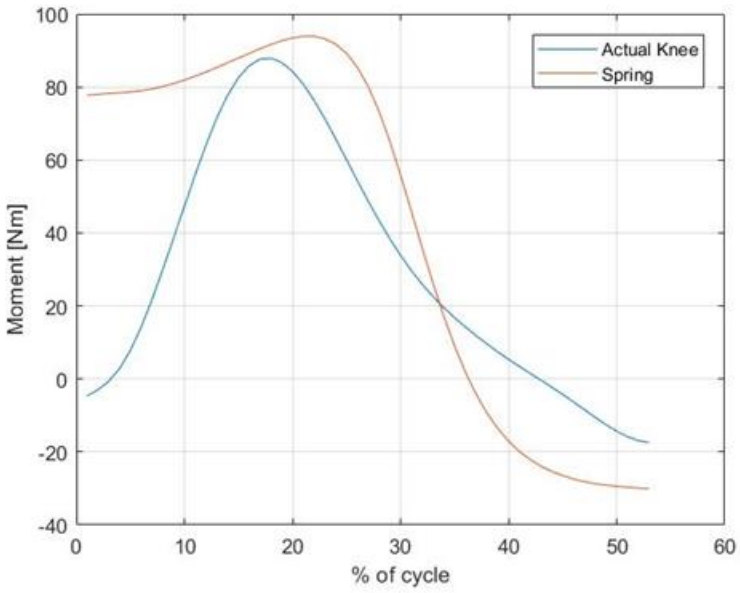

Figure 3.1.3.2 Torque comparison between biological knee joint [2] and exoskeleton during stair ascent

3.1.4. Swing and Push-Off Springs

One of the most important motion of knee is swing motion during gait. After toe off, knee must perform the swing motion so the foot doesn't hit the ground. In order to mimic the swing motion, a spring is mounted on the exoskeleton. This spring must be loaded until the toe off so it can use this energy to pull the shank back after toe off.

To be able to load this spring, a pulley and rack-pinion mechanism is used. Figure 3.1.4.1 depicts the mechanism that is designed for swing motion. Pulley rotates around ankle joint and the ratio between pulley and pinion gear is 1:7. Besides the step length of rack and pinion is 3.14 mm.

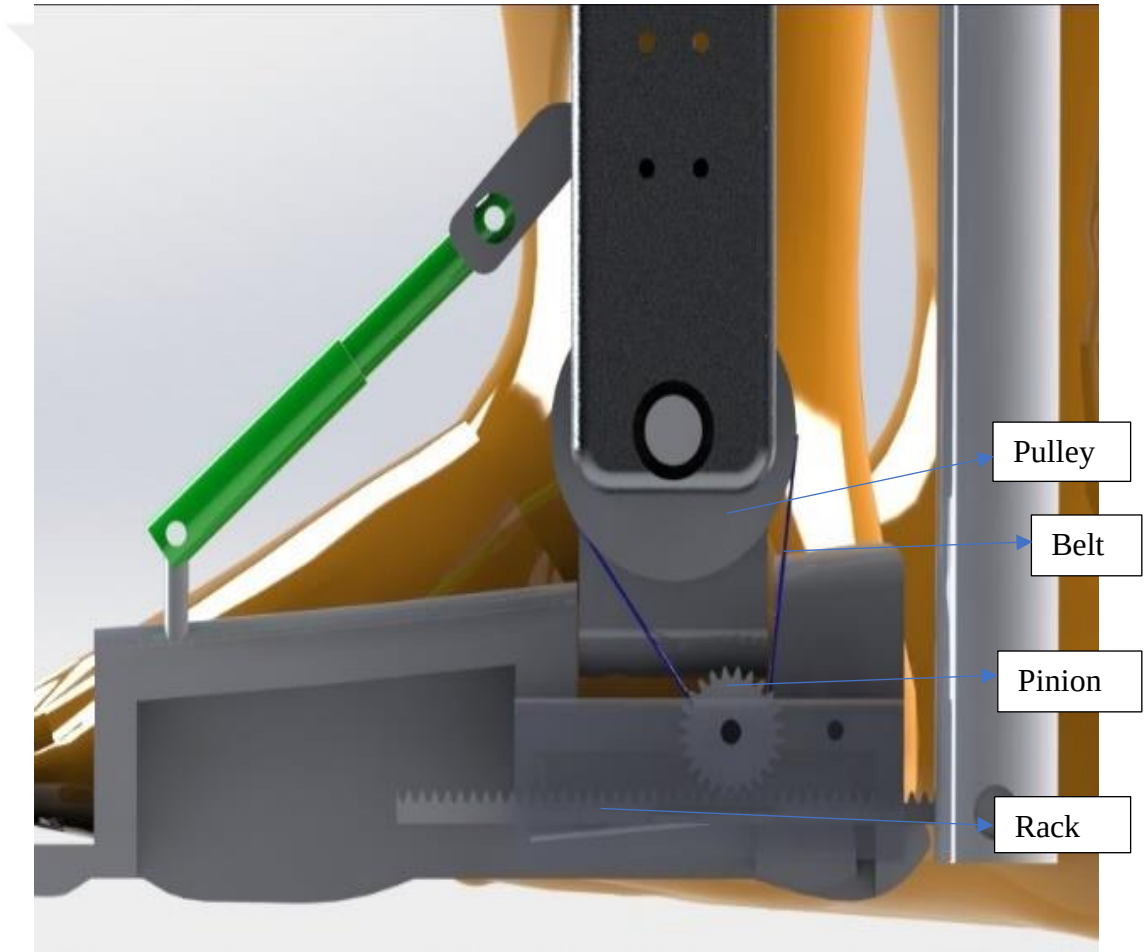

Figure 3.1.4.1 Pulley and rack-pinion mechanism

Kinematic figure and matlab codes that are used for calculations of swing and push-off spring can be seen in appendix 3.1.4. Figure 3.1.4.2 depicts the elongation vs.

force graph of knee. Slope of the red line represents the coefficient of spring used for swing motion.

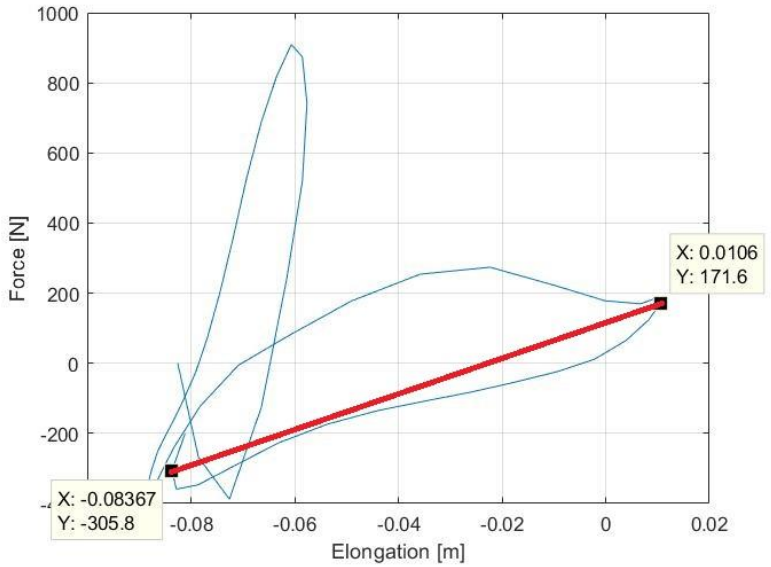

Figure 3.1.4.2 Elongation vs. force graph for swing spring

$$k_{swing} = \frac{171.6 - (-305.8)}{0.0106 - (-0.08367)} = 5064\ [N/m] \qquad (3.1.4.1)$$

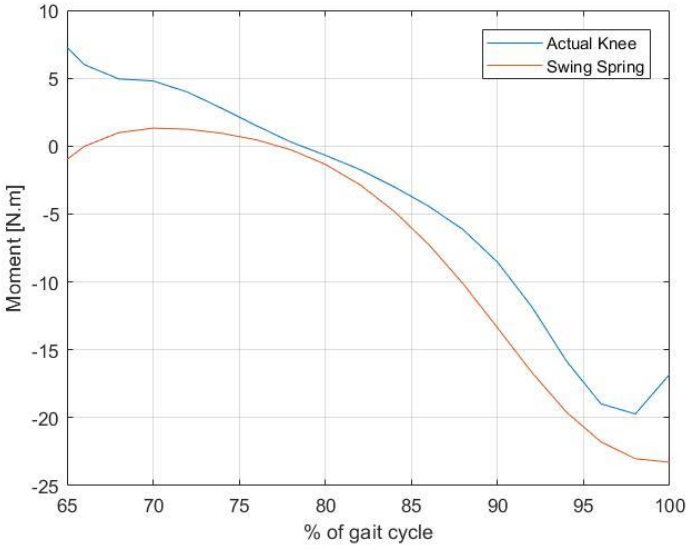

Figure 3.1.4.3 Moment comparison of actual knee and spring during swing

Figure 3.1.4.3 depicts the moment comparison of actual knee and swing spring mounted on the exoskeleton. It can be seen that spring mimics the actual joint data very

closely. Difference is resulted by the usage of linear spring while real joint shows non-linear behaviour.

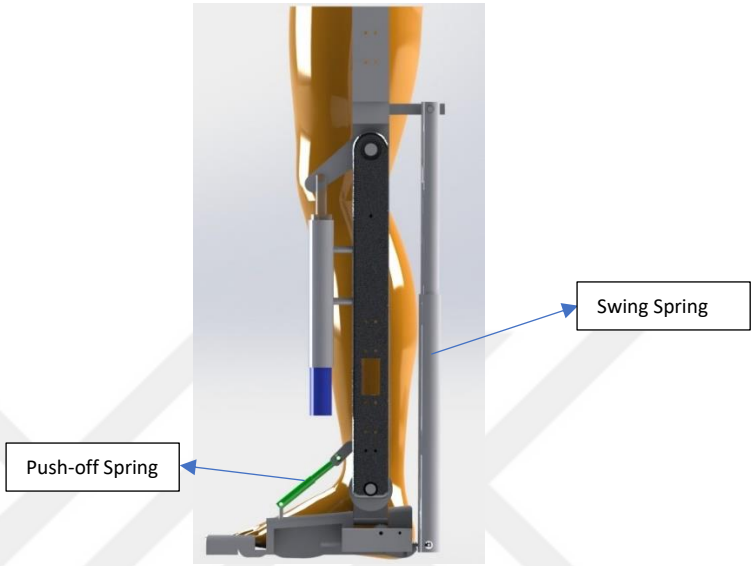

Figure 3.1.4.4 Push-off and swing springs

There are two power bursts during walking. One of these bursts is carried out by the knee joint during weight acceptance and the other one is done by the ankle joint during push-off phase. Push-off motion occurs between approximately 40-60% of stride. It is highly important to determine the spring coefficient in order to assist the push-off properly and safely. Figure 3.1.4.5 depicts the swing and push-off springs.

To do this, we generate the force data that is needed to produce the ankle torque vs. elongation of elastic element plot in Figure 3.1.4.5. In order to determine the spring coefficient, the slope of the red line has been computed. Besides, swing spring is taken into account while calculating the push-off spring becuase the swing spring is active during push-off.

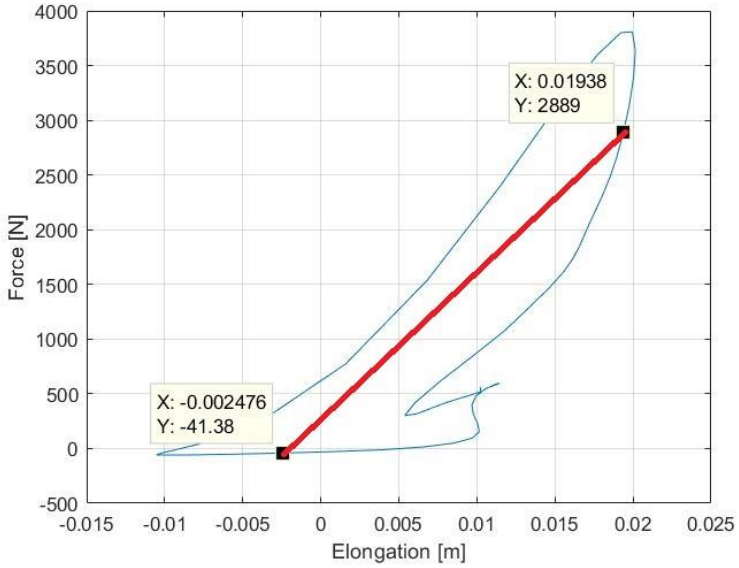

Figure 3.1.4.5 Identifying elastic constant of push-off spring from natural ankle data

$$k_{push-off} = \frac{2889 - (-41.38)}{0.01938 - (-0.002476)} = 134000\ [N/m] \qquad (3.1.4.2)$$

3.1.5. Weight Acceptance Mechanism

The motion of the knee joint was explained in section 2.4.1. The knee joint has two flexion and two extension motions in one step of walking. The first flexion starts with the heel strike in order to accept body weight. Then extension occurs so that the body can move forward (lifting up the weight). This first flexion-extension motion is called weight acceptance. The second flexion occurs just before the toe-off. The reason for this second flexion is to lift the leg in the air so that the foot do not touch or hit the ground during the swing phase. There is a weight acceptance spring mounted on the exoskeleton presented in this thesis so that the weight acceptance is carried out. But this spring inhibits the second flexion motion because the stiffness of the spring is too high for knee joint to perform the second flexion motion. In order to solve this problem, an engage-disengage mechanism must be designed.

To be able to engage-disengage the spring, touching of the foot to the ground must be sensed. So the spring must be engaged when the foot is on the ground. When it happens, spring engages and can carry out the weight acceptance. And the spring must be disengaged in the swing phase (while the foot does not touch the ground) so that the spring does not block the flexion during swing phase.

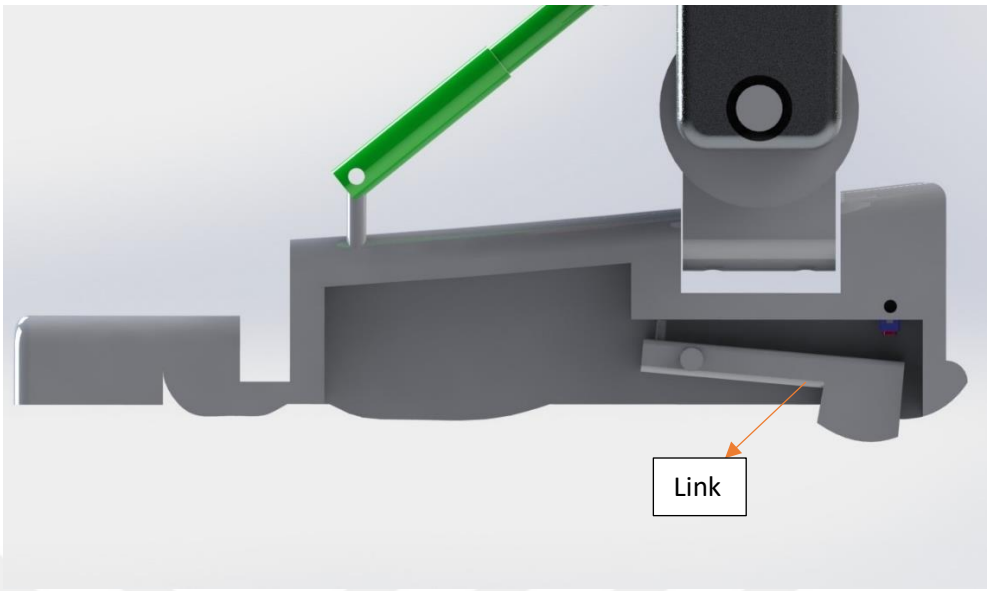

a)

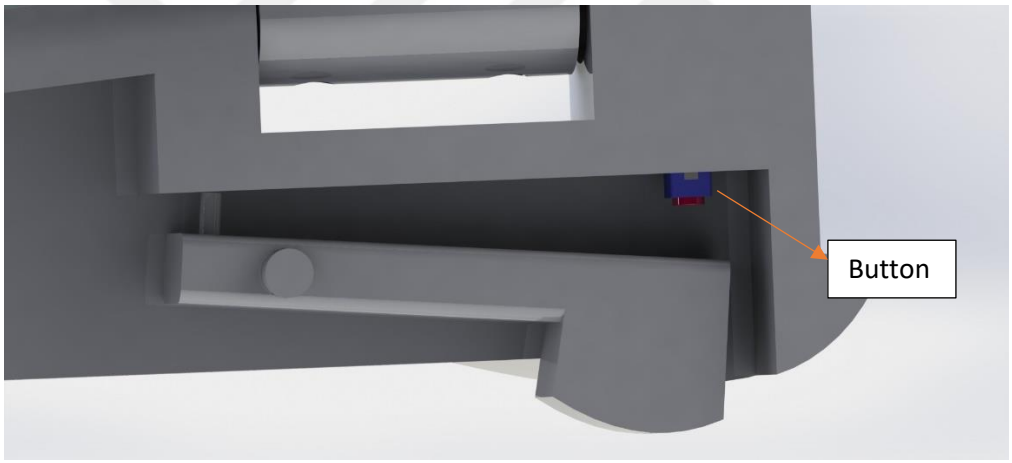

b)

Figure 3.1.5.1 A simple weight acceptance mechanism

Figure 3.1.5.1 depicts the weight acceptance mechanism mounted on the exoskeleton. When the heel touches the ground, the link goes up and presses the button which is an on-off switch. Then the button sends signal to the controller and controller locks the motor and the spring can be compressed. When the foot is in the air (swing phase), the link does not press the button, thus the motor moves freely. Figure 3.1.5.2 depicts the on and off conditions of the weight acceptance mechanism.

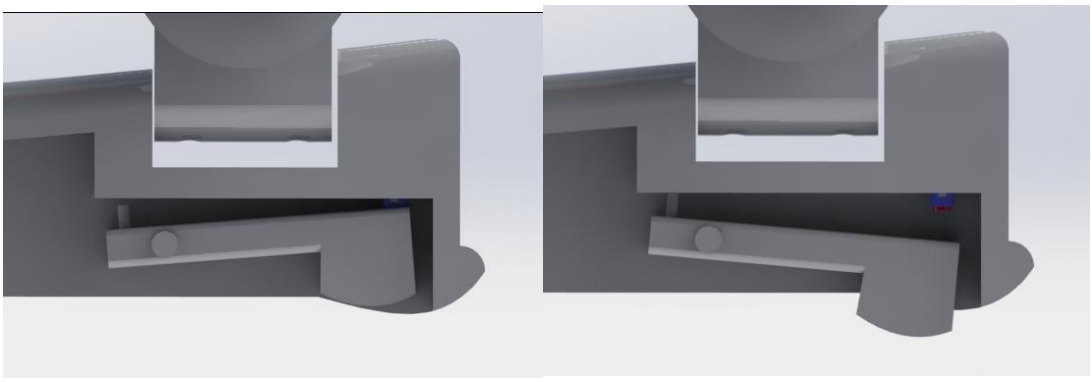

a) b)

Figure 3.1.5.2 The on (a) and off (b) positions

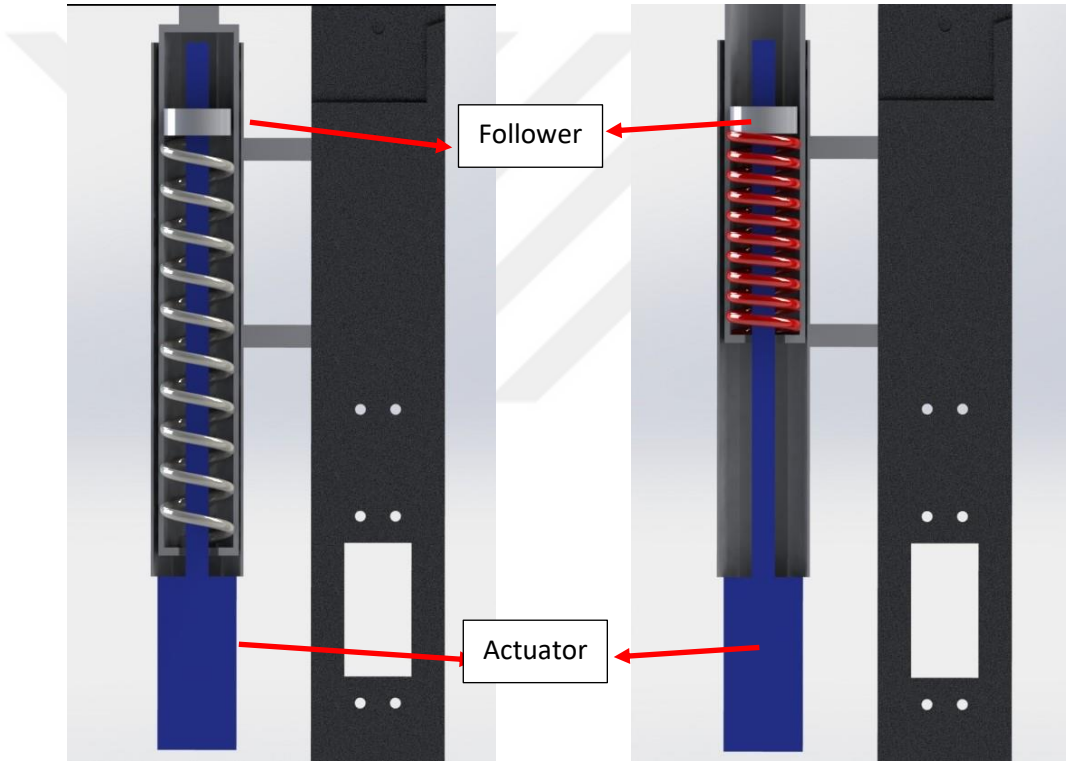

a) b)

Figure 3.1.5.3 Initial (a) and engaged (b) positions

Figure 3.1.5.3 demonstrates the initial and engaged conditions of the spring. When the button mounted on the foot is pressed, the controller locks the actuator, thus the follower does not move and spring can be compressed so that this compression energy can be used in the late phase of weight acceptance. On the other hand, follower can move freely on the ballscrew during swing phase because of the button is released. So, the spring becomes free and the swing phase is not inhibited.

3.1.6. Results and Discussion of Exoskeleton

When simulating the exoskeleton with the WA spring during walking, the system can mimic the knee joint as it is shown in Figure 3.1.6.1-a, which makes the comparison of knee joint and knee exoskeleton torque during WA. Also Figure 3.1.6.1-b depicts the power comparison of actual knee and attached spring.

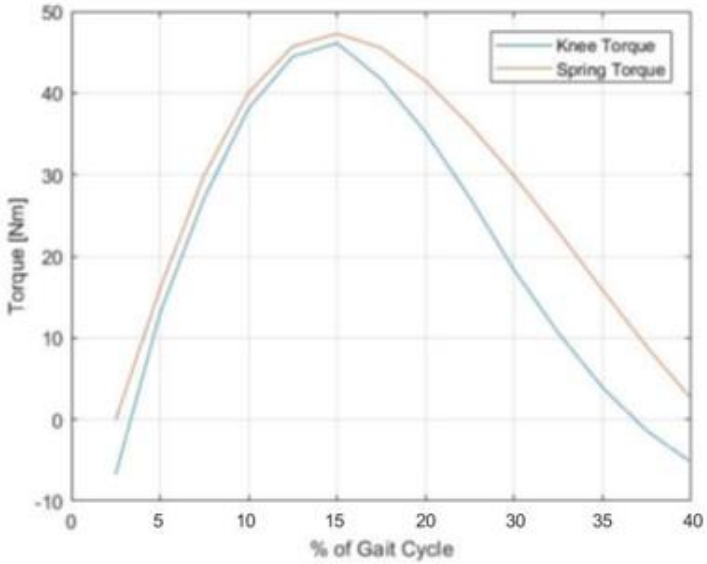

a)

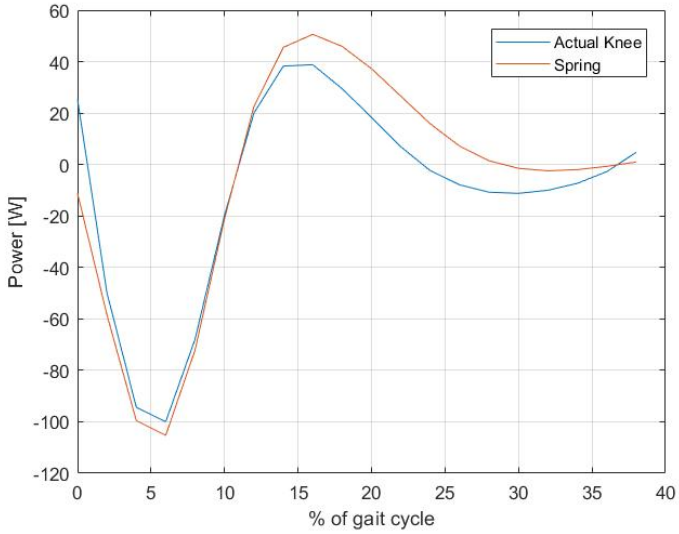

b)

Figure 3.1.6.1 Comparison of natural knee joint and exoskeleton a) torque and b) power during WA

Similar behavior is also observed when simulating the exoskeleton during sit to stand motion, which is shown in Figure 3.1.6.2 as a comparison of knee joint and knee exoskeleton torque during sit to stand motion. The reason for the difference between the knee joint and the exoskeleton torque would be due to the linearization of the force-elongation curve for the sit to stand motion.

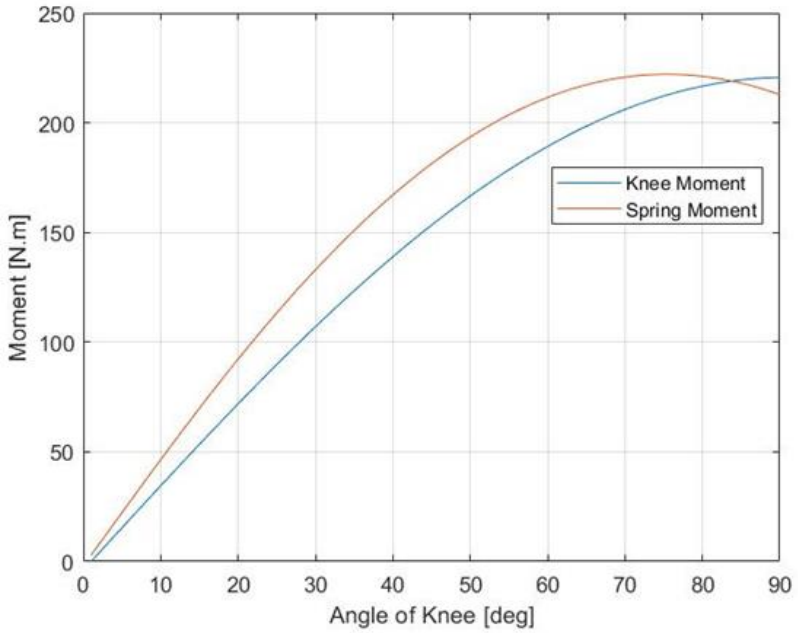

Figure 3.1.6.2 Comparison of the knee joint and exoskeleton torque during sit to stand

The comparison of knee joint and exoskeleton torque and power plots during stair ascent motion is depicted in Figure 3.1.6.3. Here, the moment of natural knee joint starts from 0 Nm, yet the initial moment of exoskeleton is nearly 80Nm. It means that the actuator has to compress to spring because of the kinematic restrictions. Then it releases the spring and after 20% motor does not have to apply power. So the spring is supportive to raise the body, which can be seen as the power reduction in Figure 3.1.6.3-a. Actuator consumes power until 20% then required power decreases to nearly zero, since spring does the job after 20% of the cycle. After 40% of cycle, spring restricts the swing motion due to the kinematics of our design. To be able to avoid this, the design includes an engage-disengage mechanism to engage the spring only between 0-40% and disengage the spring 40-100% so that the actuator does not consume unnecessary power. Because of the spring only works between 0-40% of gait cycle, only this part was plotted.

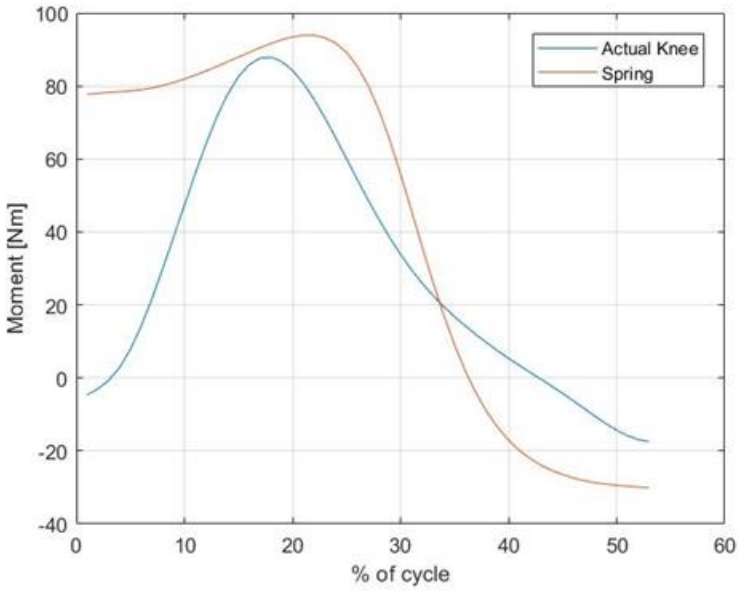

a)

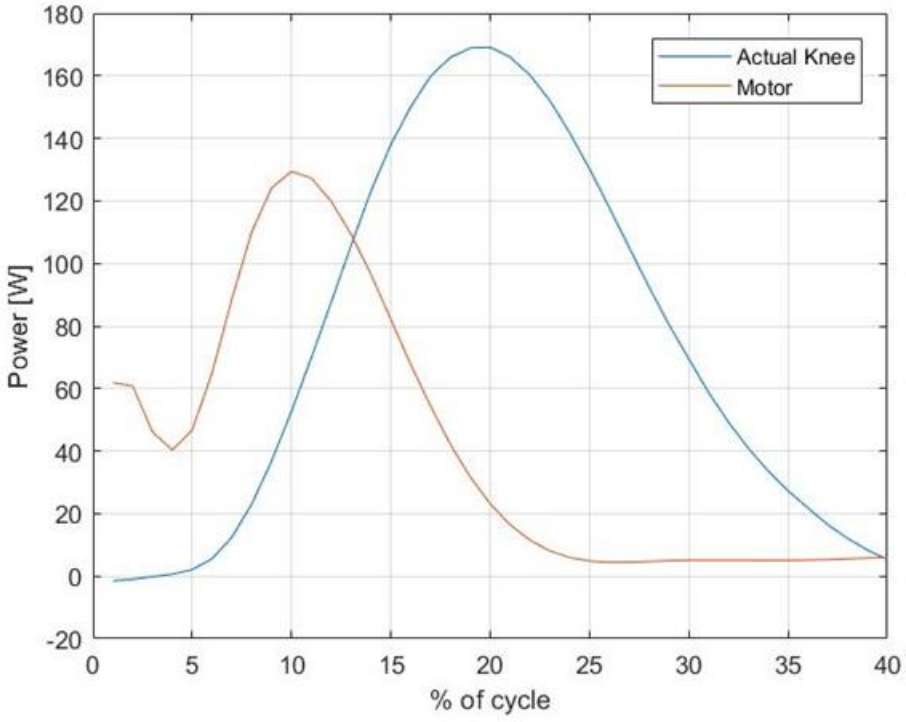

b)

Figure 3.1.6.3 a) Moment and b) Power plots of knee during ascending

Figure 3.1.4.3 depicts the moment behaviour of swing spring and actual knee joint. One can easily say that the pattern swing spring follows and the moment values are very

close to actual data. There is slight difference between spring and actual data which is occured because of the linear spring is used to perform the task while knee joint doesn't behave like linear spring.

The complete CAD of the proposed exoskeleton design is presented in Figure 3.1.6.4 as it is attached to human leg.

Figure 3.1.6.4 3D CAD model of exoskeleton design

3.2. Test Bed Design

3.2.1. Center of Mass (CoM) Analysis

In order to design a test platform, data of the center of mass displacement and the hip joint angles were examined. First, for the translation of the center of mass in sagittal plane, data gathered from [20] was analyzed.

It can be easily seen in Fig. 6 in [20] that CoM displacement motion is cyclic motion with approximately 30 mm amplitude. So, we designed a cam to produce this CoM motion. Figure 3.2.1.1 depicts our cam design. Besides, one revolution of cam corresponds to one step. In Figure 3.2.1.2, one can see CoM displacement when the cam is implemented into the system. Amplitude of motion matches with the data of healthy

person's CoM data. Power consumption of the motor actuating the cam can be found by using

$$P = F * v \tag{3.2.1.1}$$

where m is the mass of the upper body which is 50 kg for 75 kg person and v is velocity of the CoM. Singleton et. al. stated that one step takes place in 1.45s in symmetrical walking [35]. It means the CoM must travel 120 cm in 1.45 seconds So, the power consumption is

$$P = 50 * 9.81 * \frac{0.12}{1.45} = 40.5W \tag{3.2.1.2}$$

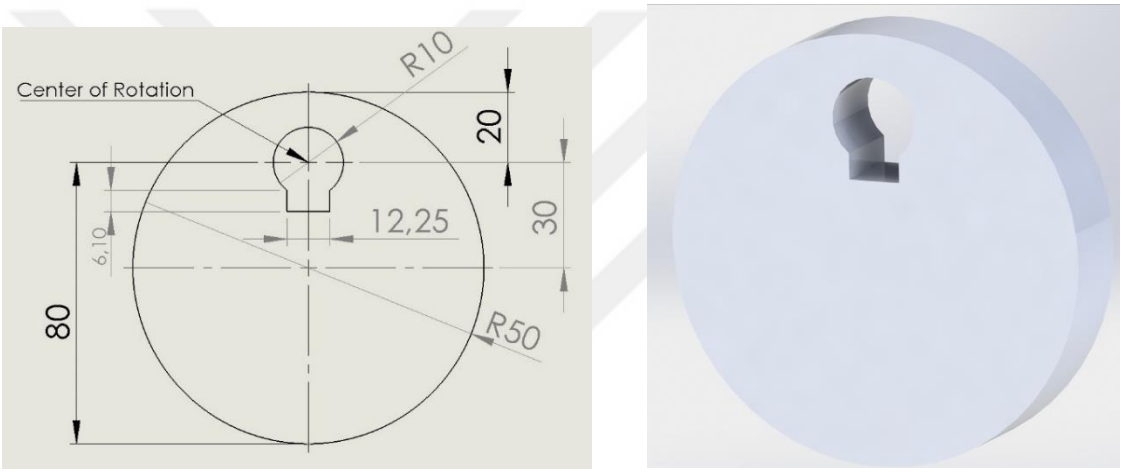

a) *b)*

Figure 3.2.1.1 Cam Profile a) Technical Drawing of Cam, b) 3D Model of Cam

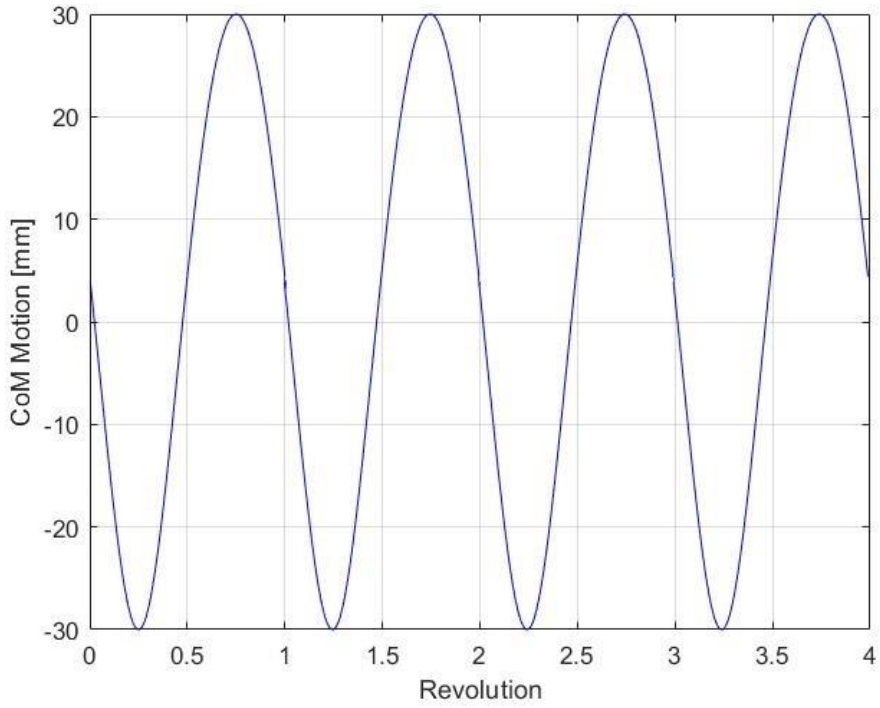

Figure 3.2.1.2 CoM Motion With Cam

Yet, the cam mechanism has a major handicap which is not avaliable for different speeds of walking. In [36], it is seen that amplitude of the CoM displacement changes with the speed of walking. But, when there is a cam mounted on the test bed to produce CoM motion, it becomes highly difficult to adapt the system to different speed levels or changing speeds while walking. Because of that vital reason, a ballscrew with an actuator was chosen to actuate the system. Because amplitude and the speed of the CoM can be controlled with the actuator in a relatively easier manner. This actuator with ballscrew will be discussed in the control section.

3.2.2. Hip Data Analysis

Secondly, hip data gathered from [26] was examined to be able to determine which system is going to be used for the test bed platform. Figure 3.2.2.1 shows the angles of hip during walking at normal speed. The hip has the most homogenuous angle change among three joints. It starts its motion at nearly 20° and extension occurs until the hip angle arrives to -20°. This extension motion corresponds to the part between heel contact and toe off (0-60%). Then the hip starts its flexion motion until it reaches +20°.

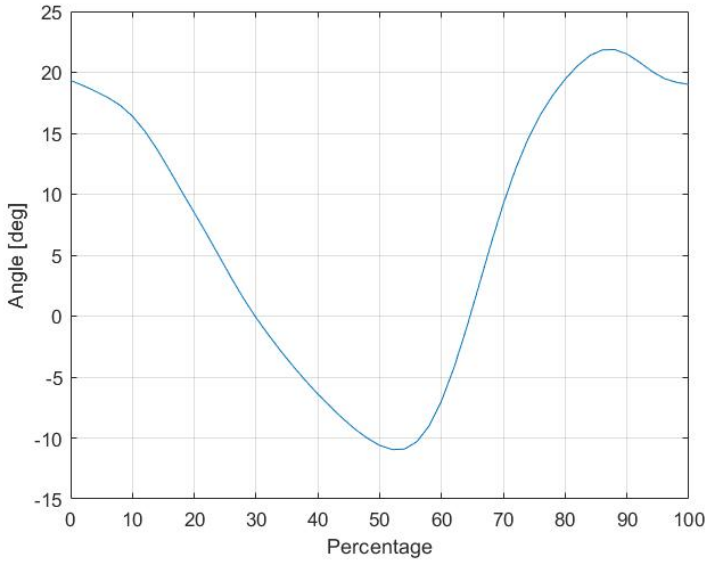

Figure 3.2.2.1 Angles of Hip During Normal Walking

The hip joint starts its motion with moment boost (0-5%). This sudden increase in moment is caused by the impact of heel strike. Then the moment starts to decrease to zero (nearly 20% percent of gait) and it increases in negative direction. The reason of changing the direction of moment is that the distance between the foot and hip in the horizantal direction. After 20% of gait, this distance increases until the toe-off occurs. After toe-off (60%), hip moment starts increasing so that the leg swings. Hip angle increases until nearly 95% of gait then it decreases about 3-4 degrees. This decrease causes hip moment ecrease between 95-100% of gait. Figure 3.2.2.2 shows the moment behaviour of the hip.

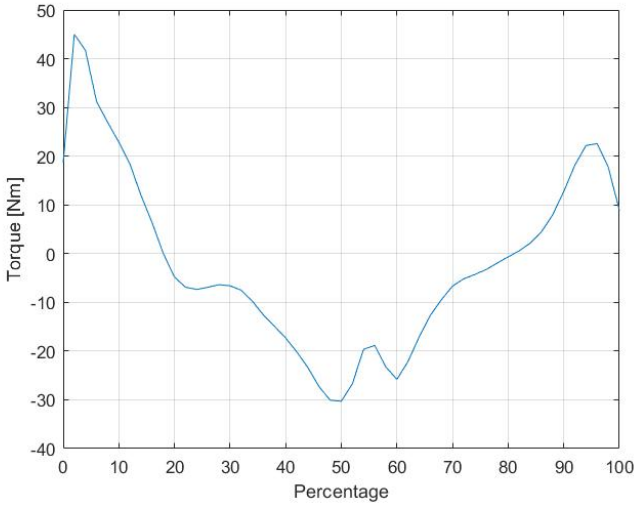

Figure 3.2.2.2 Hip moment in one single step

3.2.3. Design

We compared three designs in order to reduce the actuation torque required to actuate the thigh. These concepts are direct drive, fourbar mechanism and fourbar with torsion spring mechanism. These concept designs are depicted in Figure 3.2.3.1.

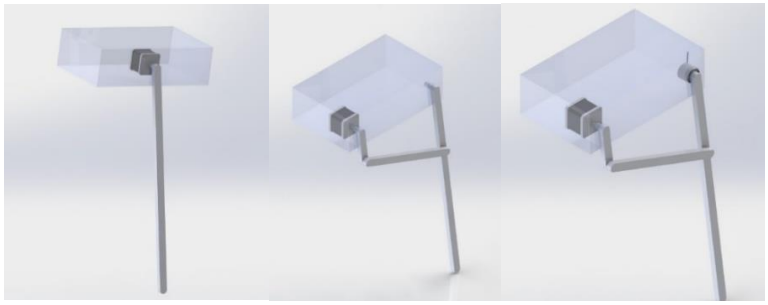

a) b) c)

Figure 3.2.3.1 Concept Designs a) Direct Drive b) Fourbar Mechanism c) Fourbar with Torsion Spring Mechanism

First we examined the direct drive. For the direct drive, torques and angles are the same with the actual data of hip joint. Then we designed a fourbar mechanism to be able to reduce the motor torque. First, Autolev program was used to obtain the kinematic equations for four-bar. These codes can be seen in the appendix. Then the kinematic equations obtained from Autolev were substituted in MATLAB codes so that the kinematic calculations can be performed via MATLAB. After this step, we implemented a torsion spring to the system. The spring constant of this torsion spring is calculated from hip joint angle-torque graph. The spring constant of the torsion spring is 1.2157 [Nm/deg] or 69.65 [Nm/rad] which corresponds to the slope of the red line in Figure 3.2.3.2.

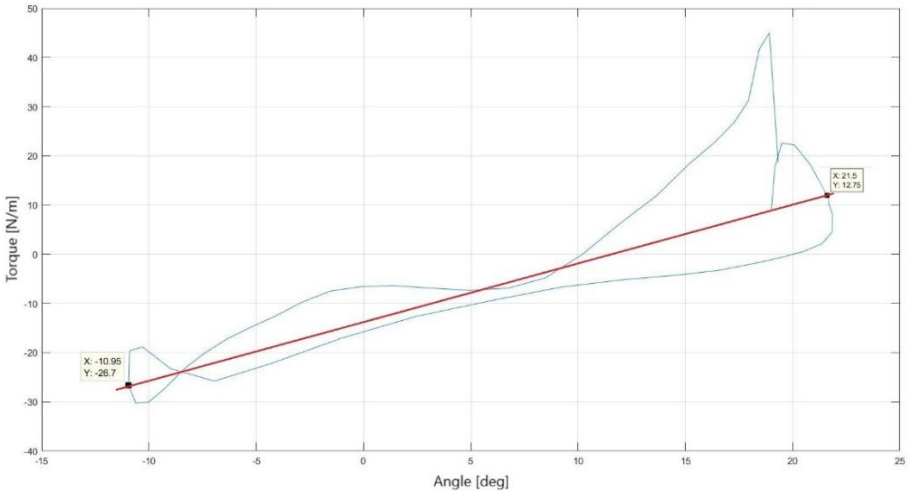

Figure 3.2.3.2 Torque Angle Graph of Hip

We can see the torque difference between direct drive and four bar mechanism. The torque required to actuate the thigh is reduced to approximately 30% of its actual torque. But when we have reduction on torque, the workspace of the mechanism is increased. While the direct drive motor works between +20° and -10°, actuator of four bar operates between nearly +36° and -30°.

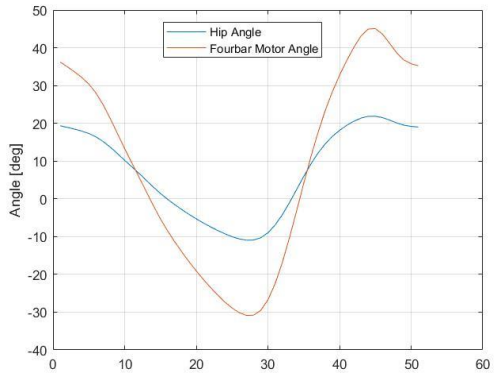

a)

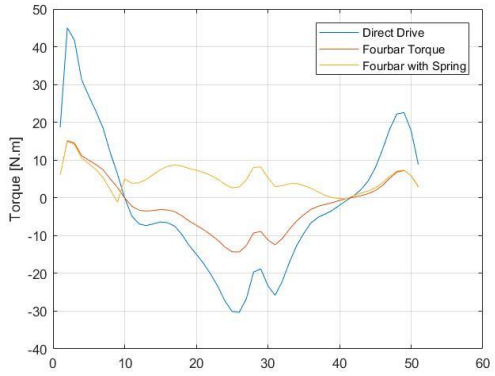

b)

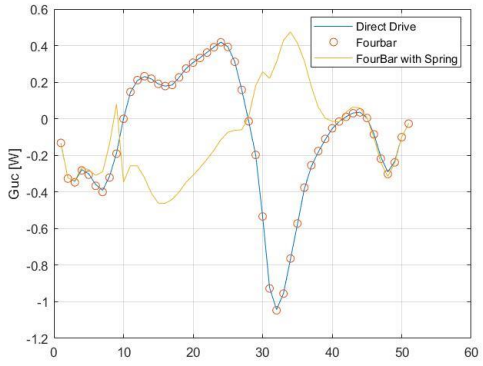

c)

Figure 3.2.3.3 Comparison Graph in terms of a) Angle b) Torque c) Power

a)

b)

Figure 3.2.3.4 Concepual design of test bed a) Test bed with cam b) Test bed with ballscrew

Chapter 4

Control

4.1 Control of Center of Mass (CoM)

To be able to control the center of mass of the test bed, data gathered from [20] was analyzed. It can be easily seen that human CoM motion in normal walking is approximately a sinusoidal motion with 30 mm amplitude in horizantal direction.

First we need to obtain the equation of motion of CoM. Lagrange equation is used to obtain the equation of motion [37]. Figure 4.1.1 depicts the representation of center of mass of 75 kg of an average male.

$$\frac{\mathrm{d}}{\mathrm{dt}}\left(\frac{\partial \mathrm{L}}{\partial \dot{\mathrm{q}}_{\mathrm{i}}}\right) - \left(\frac{\partial \mathrm{L}}{\partial \mathrm{q}}\right) = \mathrm{Q}_{\mathrm{i}} \tag{4.1.1}$$

where the terms of $\dot{q}_i$ and q are variables of the system. Because of the CoM moves in horizontal direction, variables of this system are $\dot{y}$ and y which are velocity and position, respectively. Besides Q_i actuation parameter such as torque, force etc.

$$L = E_{Kinetic} - E_{Potential} \tag{4.1.2}$$

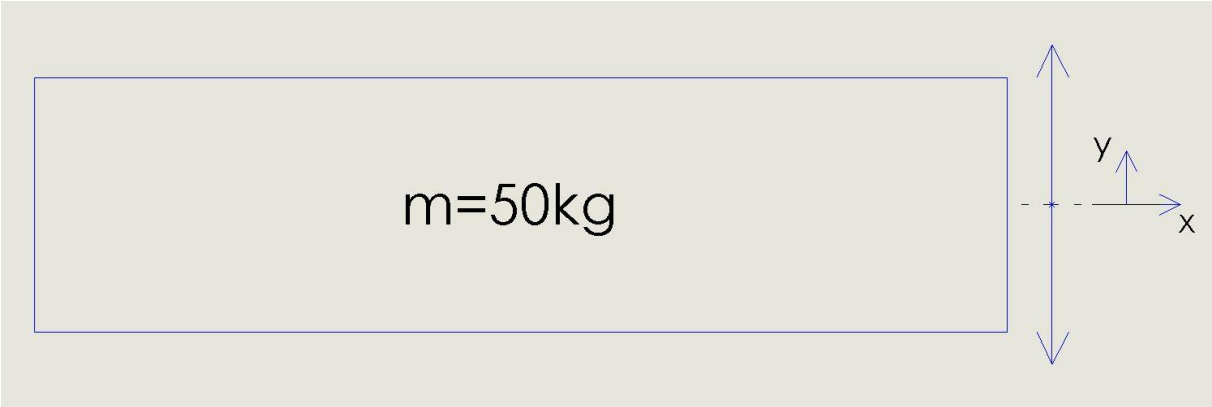

Figure 4.1.1 Representation of CoM

In order to operate the Lagrange equation of motion, first we need to find the L term which equals to subtraction of potential energy from kinetic energy. So that;

$$E_{kinetic} = \frac{1}{2}mv^2 \tag{4.1.3}$$

V is velocity of CoM and it equals to first time derivative of position which is y. We can easily find the first time derivative of y as;

$$\frac{dy}{dt} = \dot{y} \tag{4.1.4}$$

So the kinetic energy of the system is;

$$E_{kinetic} = \frac{1}{2}m\dot{y}^2 = \frac{1}{2}50\dot{y}^2 = 25\dot{y}^2\ [Joule\ ] \tag{4.1.5}$$

And the potential energy of the system is;

$$E_{potential} = mgh = 50 * 9.81 * y = 490.5y\ [Joule\ ] \tag{4.1.6}$$

So the L term becomes

$$L = 25\dot{y}^2 - 490.5y\ [Joule\ ] \tag{4.1.7}$$

Now the Lagrange equation can be performed.

$$\frac{d}{dt}\left(\frac{\partial(25\dot{y}^2 - 490.5y)}{\partial\dot{y}}\right) - \left(\frac{\partial(25\dot{y}^2 - 490.5y)}{\partial y}\right) \tag{4.1.8}$$

$$= 50\ddot{y} + 490.5$$

$$50\ddot{y} + 490.5 = F \tag{4.1.9}$$

In order control this system, PID controller was used. First we need to transfer the equation (4.1.9 into frequency domain with Laplace Transformation [38] which gives

$$ms^2Y(s) - sy(0) - sy'(0) = F(s) - \frac{490.5}{s} \tag{4.1.10}$$

Since initial conditions are zero and $\frac{490.5}{s}$ term at right side of the equation can be considered as disturbance, the equation becomes

$$ms^2Y(s) = F(s) \tag{4.1.11}$$

Which leads to transfer function

$$\frac{Y(s)}{F(s)} = \frac{1}{ms^2} \tag{4.1.12}$$

Figure 4.1.2 depicts the simple PID control of a system. Subtraction of output from reference signal is error signal of the system. The PID controller perform the control to be able to decrease the error to zero by means of k_p(proportianal gain), k_i(integral gain) and k_d(derivative gain). To be able to find the coefficients block diagram of the system needs to be simplified.

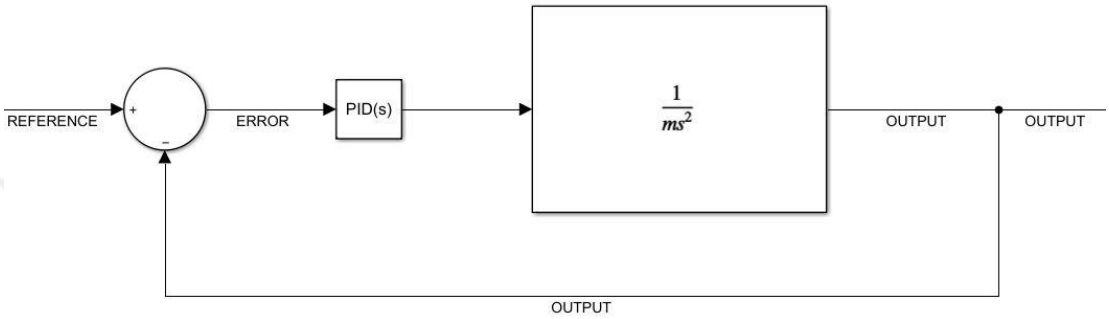

Figure 4.1.2 Simple representation of PID control system

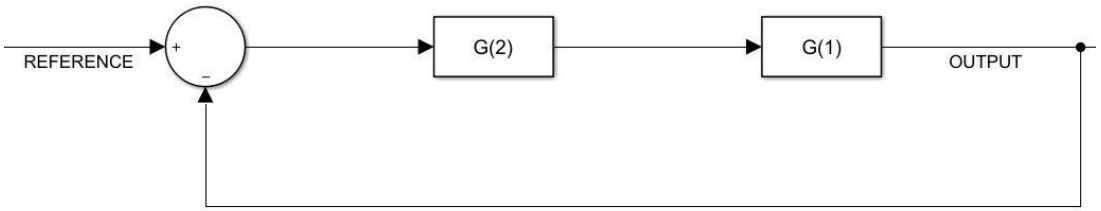

Figure 4.1.3 A simple block diagram

In Figure 4.1.3, a simple block diagram is demonstrated. Rule of simplification of the block diagram [39] for this condition gives $\frac{G_1 G_2}{1+G_1 G_2}$. By using this rule, our system is simplified into

$$\frac{PID}{ms^2 + PID} \tag{4.1.13}$$

The term PID equals to $k_p + \frac{k_i}{s} + k_d s$ [40]. So, the denominator of the new transfer function becomes

$$s^2 + \frac{k_p}{m} + \frac{k_i}{ms} + \frac{k_d s}{m} = 0 \tag{4.1.14}$$

This system is a second order system. The standart equation of motion for the second order system is

$$s^2 + 2\xi w_n s + {w_n}^2 \tag{4.1.15}$$

where ξ is the damping ratio and $w_n$is the natural frequency of the system. Thus the final equation becomes

$$s^2 + \frac{k_p}{m} + \frac{k_i}{ms} + \frac{k_d s}{m} = (s^2 + 2\xi w_n s + {w_n}^2) \tag{4.1.16}$$

In order to match the terms, an s term with a pole must be added to the standart equation of motion. So the equation becomes

$$s^3 + \frac{k_p s}{m} + \frac{k_i}{m} + \frac{k_d s^2}{m} = (s + p_0) * (s^2 + 2\xi w_n s + {w_n}^2) \tag{4.1.17}$$

where p_0 is the root that is added which is higher than zero (it is because the pole must be at the left side of the imaginary axis to keep the system stable) and it can be considered between $(2..5) * \xi w_n$ (the reason for that is the pole that is added must be at the left side of the dominant pole which is $-\xi w_n$ according to pole placement method [40]). To be able to find the PID constants (k_p, k_i and k_d), ξ and w_n must be assigned according to system requirements. Firstly ξ and w_n terms must be found. To do this, eqation (4.1.18 must be used

$$\tau = \frac{1}{\xi w_n} \tag{4.1.18}$$

where τ is the time constant and was assumed to be 0.1. Now, the term ξ must be assigned. At first, it is assigned as 1 (critically damped system). So the natural frequency becomes $w_n = 10\ Hz$. Under these circumstances p_0 equals to 30. When the expansion of the right side of the equation is done, the equation becomes

$$s^3 + \frac{k_p s}{m} + \frac{k_i}{m} + \frac{k_d s^2}{m} = s^3 + 50s^2 + 700s + 3000 \tag{4.1.19}$$

So, the coefficients of the controller can be found from the equation above as $k_p = 35000$, $k_d = 2500$ and $k_i = 150000$.

To be able to run a simulation, MATLAB/Simulink was used. Firstly, CoM system is assigned to S-Function Builder. The system has one input (force that is resulted

by the actuation of motor with ballscrew) and two output (position and velocity of CoM). Figure 4.1.4 depicts the input and output assignments in MATLAB/Simulink S-Function Builder. F in Figure 4.1.4-a is force, y and yd are horizontal position and horizontal velocity of CoM, respectively.

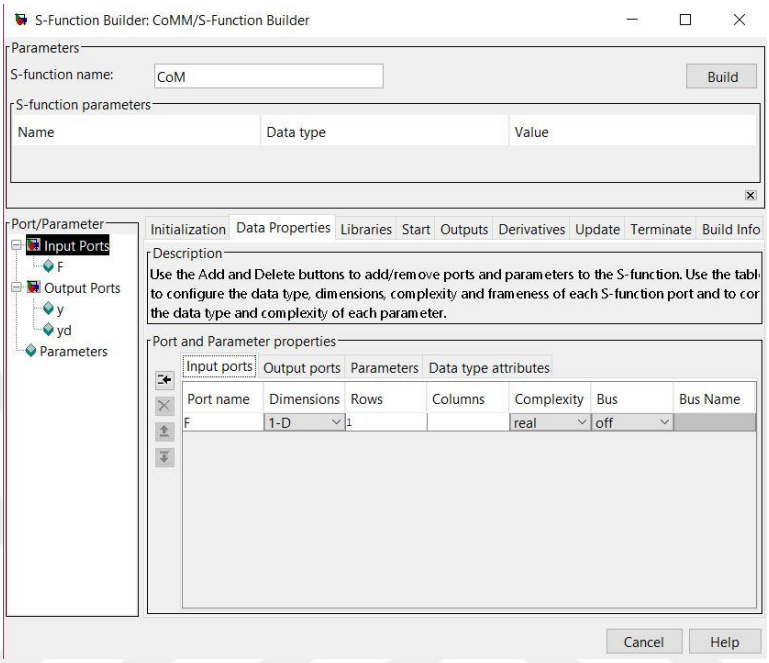

a)

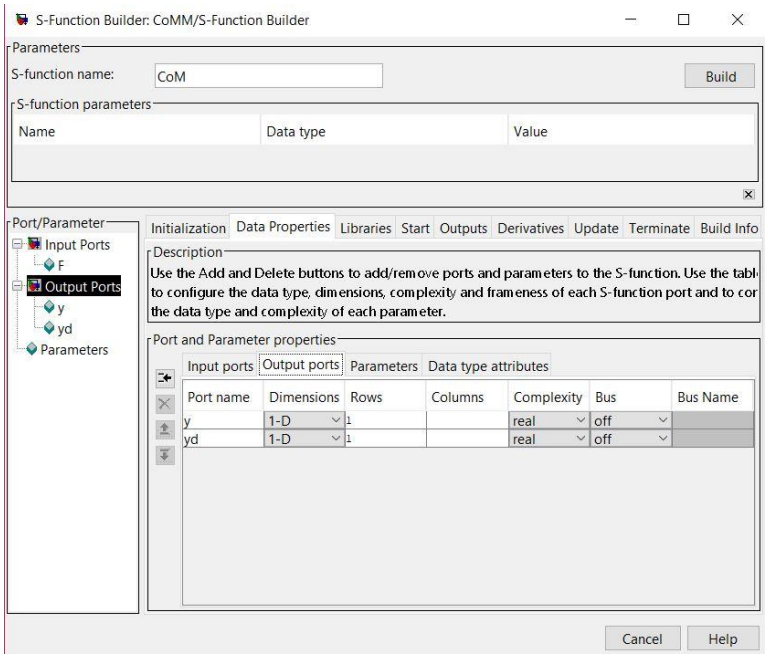

b)

Figure 4.1.4 Input (a) and output (b) assignments for S-Function Builder

Secondly, acceleration of the CoM system must be introduced into derivatives section in S-Function Builder so that the simulink can take integral of the acceleration to be able to find the position and velocity of the system. For this purpose, equation (4.1.20 is used. Figure 4.1.5 shows the derivative section. In this section, m represents the mass of the system which is 50 kg, g is gravitational acceleration (9,81 m/s^2) and ydd is the acceleration of the system.

$$ydd = \ddot{y} = \frac{F - 490.5}{50} \tag{4.1.20}$$

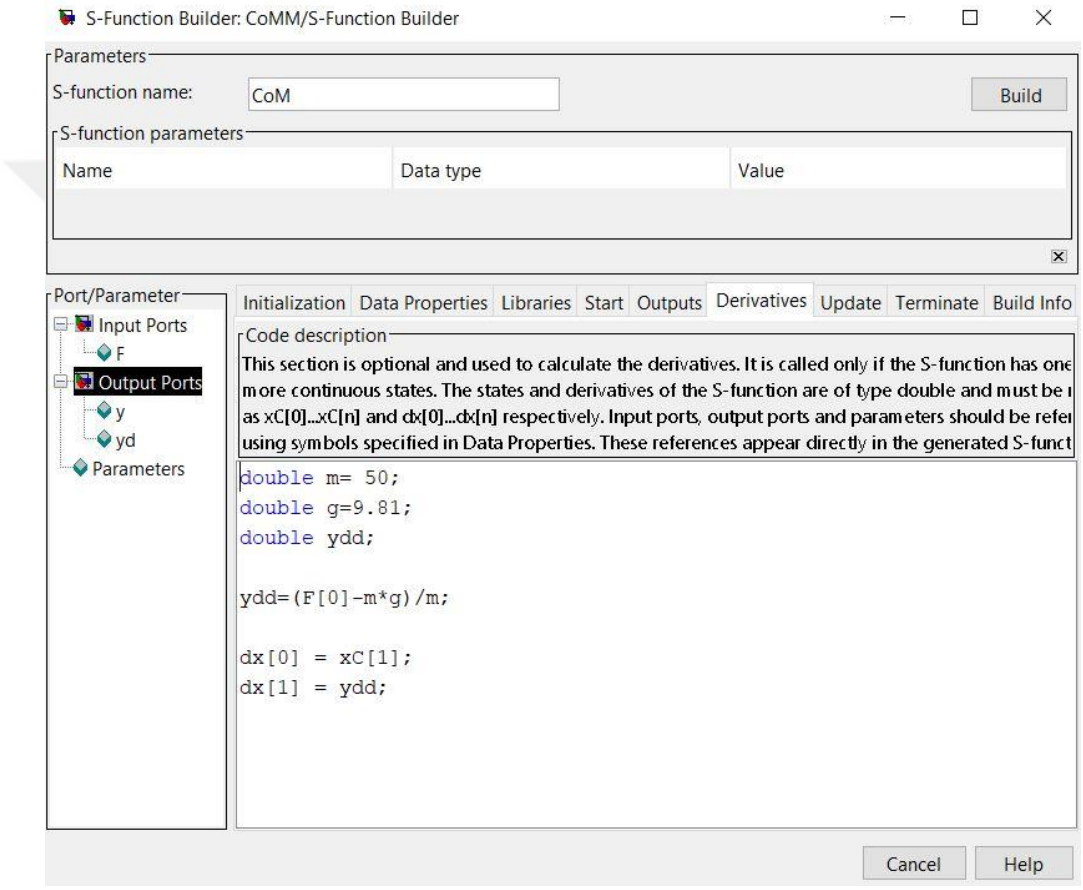

Figure 4.1.5 Derivatives section in S-Function Builder

Besides, xC[1] and ydd are first derivatives of x[0] and x[1], respectively. Due to ydd is known (from equation (4.1.20), the velocity of the system which is x[1] can be known by taking the first integral of ydd in real time simulation. Similarly, position of the system can be found by taking the integral of the velocity.

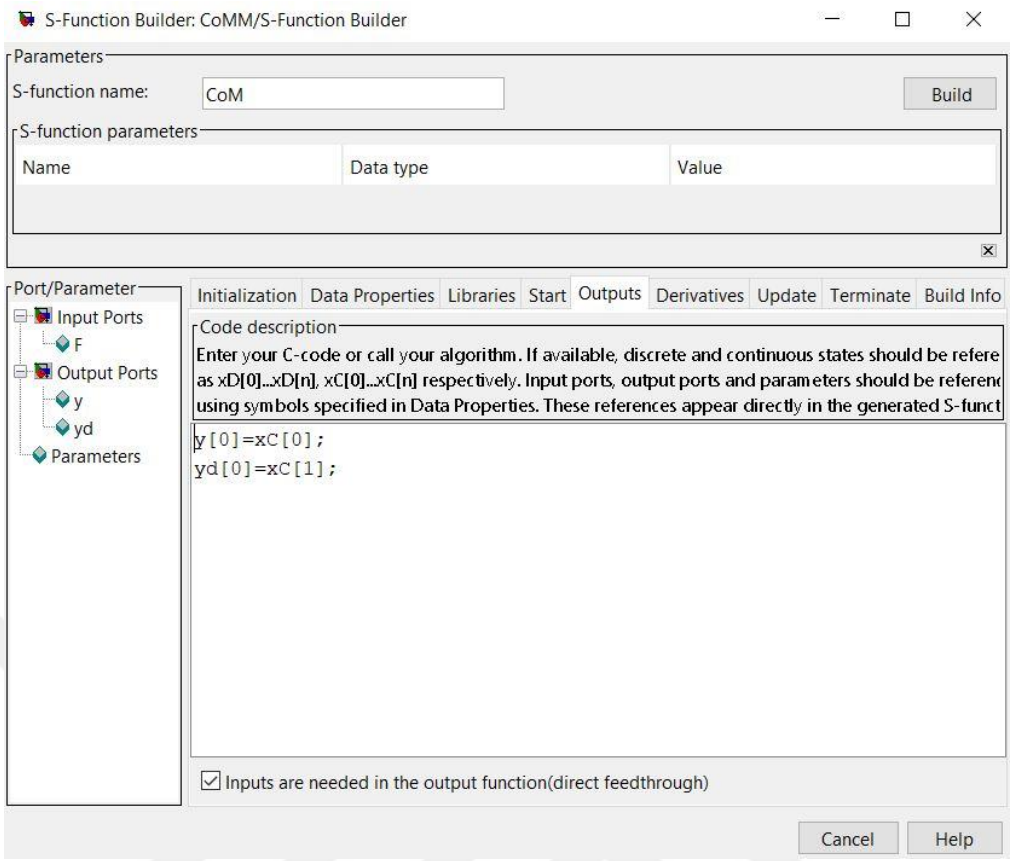

Figure 4.1.6 Outputs section of S-Function Builder

Then, outputs of the system which are y (position) and yd (velocity) must be introduced into S-Function Builder. Figure 4.1.6 depicts the outputs section of S-Function Builder. After that point, Simulink model can be built. Figure 4.1.7 shows the Simulink model of the system. A sine wave generator feeds the system with a sine wave with 0.03m amplitude because Richter et al. stated that CoM motion of a human body is a cyclic horizontal motion with 30 mm amplitude [20]. Figure 4.1.8 shows the properties of the sine wave used in the Simulink model.

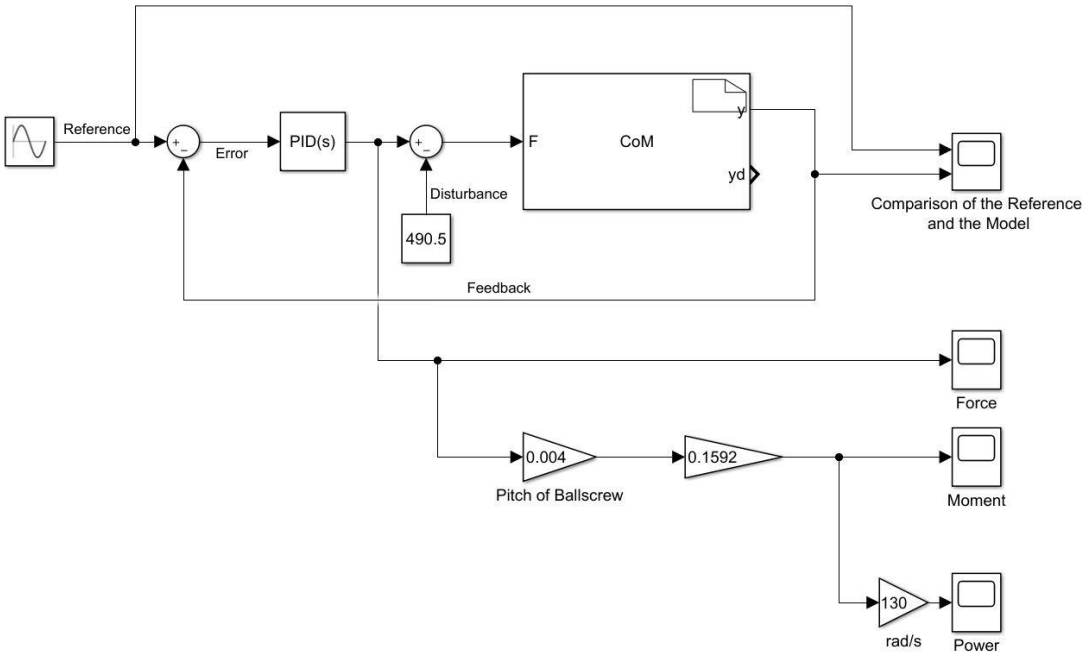

Figure 4.1.7 Simulink model of the CoM system

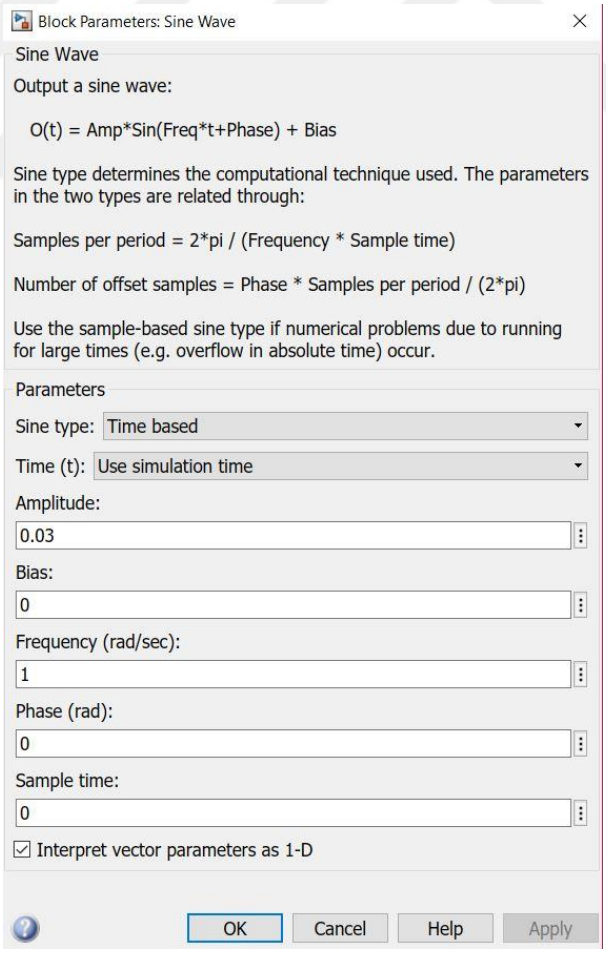

Figure 4.1.8 Sine wave generator

After feeding the system with a sine wave, the controller must be specified with the k_p, k_i and k_d constants which are 350000, 150000 and 2500, respectively. Figure 4.1.9 shows the PID parameters. Finally, the position signal that CoM model produces must be subtracted from the reference signal via sum block to be able to find the error of the system. The error signal is in meters unit while input of the CoM model has force input. This conversion is performed by the PID constants.

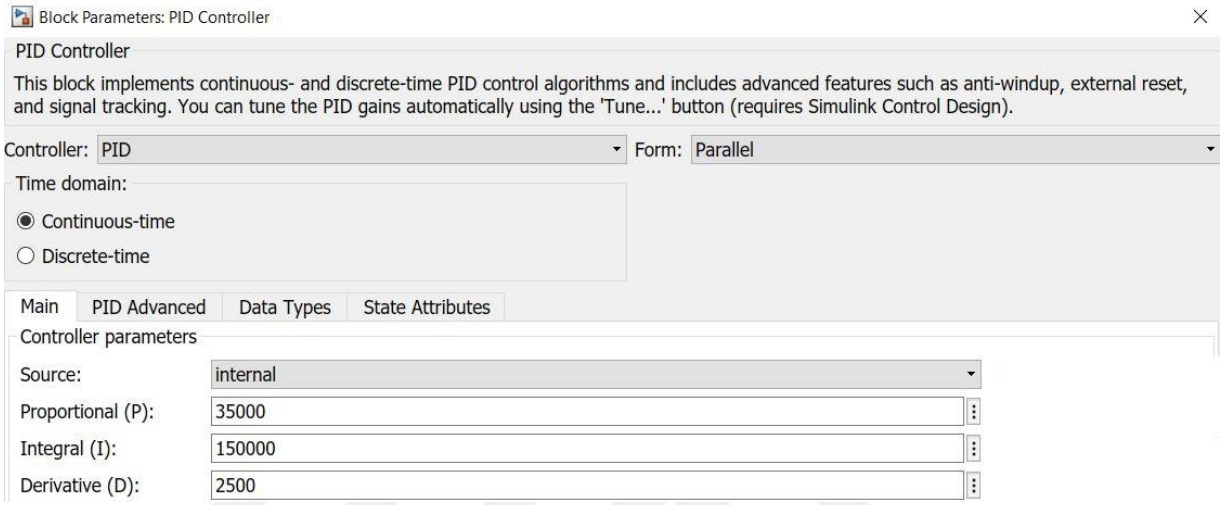

Figure 4.1.9 PID parameters

After all the blocks implemented to the model and run the simulation comparison of the model and the reference signal can be seen via scope block. Figure 4.1.10 depicts the simulation result of the model. A slight error occured at first but the controller is able to eliminate this error and make the model of CoM follow the desired trajectory.

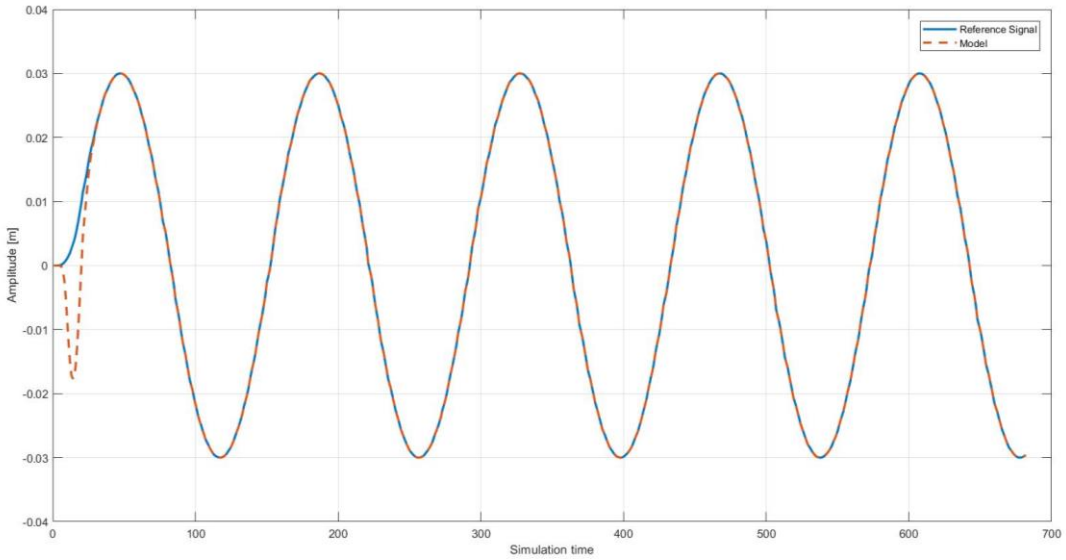

Figure 4.1.10 Result of the simulation

At first, controller is not able to follow the trajectory but after a while simulation gives very good results. It can be seen that the CoM can perform the desired motion. Besides, required force, torque and the power that the actuator must produce can also be determined via using Simulink. Required force can be scoped by connecting a scope block to the output of the PID block which also connected to input of the CoM model (F). For the required torque, equation for the ballscrew must be performed which is [41]

$$\tau = \frac{p * F}{2\pi} \tag{4.1.21}$$

p is pitch of the ballscrew which was chosen as 0.004 m. F is the required force. Besides, the 0.1592 value that is connected to find the moment (can be seen in Figure 4.1.7) represents the $\frac{1}{2\pi}$ in the equation. Furthermore, the power can be found with [42]

$$P = \tau * w \tag{4.1.22}$$

where P is required power, τ is torque and w is the angular velocity of the actuator. One cycle of the normal walking is completed in 1.45 seconds [35]. It means the ballscrew must turn 30 times (120 mm $amplitude/4$mm pitch) in 1.45 seconds. So the angular velocity of the actuator must be

$$30 * \frac{2\pi}{1.45} = 129.9 \approx 130\, rad/s \tag{4.1.23}$$

So a gain block which has magnitude of 130 is connected to find the required power.

Figure 4.1.11 demonstrates the plots of the required force, torque and the power to be able to control the CoM system on the desired trajectory. Force that actuator must supply with the help of ballscrew makes a jump to nearly 630 N and it decrease to 490 N at first. Then it stays stable around that value with some fluctuations. Torque value also makes jump to approximately 0.4 Nm and it goes down to 0.3 Nm. Finally the power value goes up to almost 53 W and it decrease to approximately 40 W. These jumps at the beginning of the plots are resulted from the error which can be seen in Figure 4.1.10. It was stated that an error occures at the beginning of the motion. Since the PID controller intends to eliminate this error, it overruns the actuator at first. So the jumps at first occur.

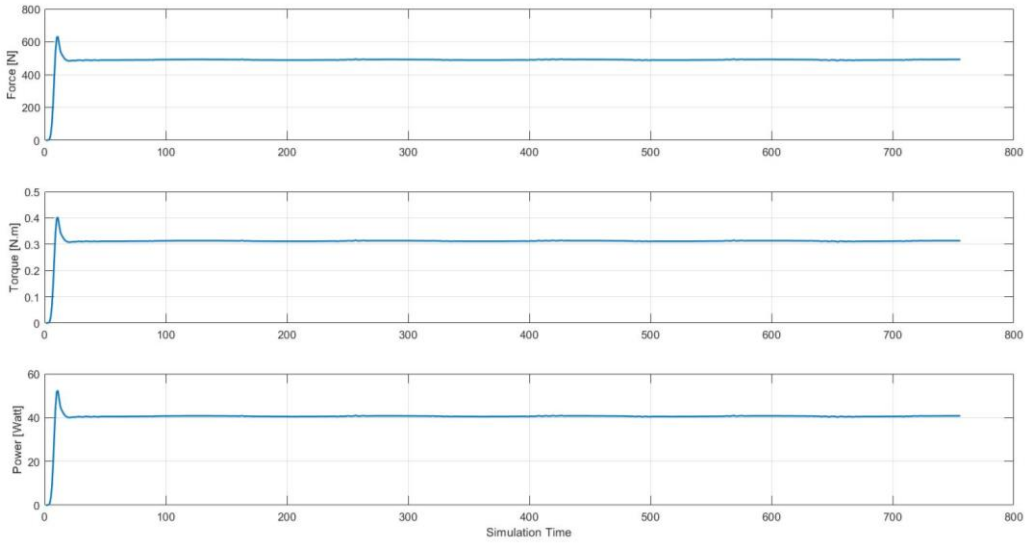

Figure 4.1.11 Required force, torque and power for the actuator

4.2 Control of The Thigh

In order to control the thigh motion, inertial effects of the second and the thigh links were neglected because masses of the links are very small and the motion is relatively slow.

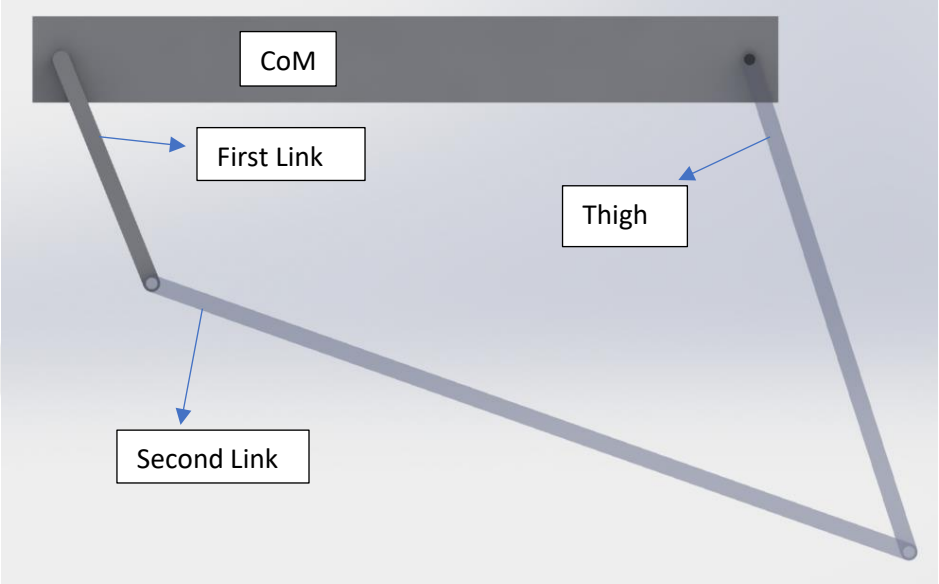

Figure 4.2.1 CoM and fourbar for thigh actuation

First, the equation of motion must be obtained with using equation (4.1.1. Kinetic and potential energy equations must be formed so that the L term can be found. Kinetic energy of the system is

$$\frac{1}{2} I \dot{q}^2 \tag{4.2.1}$$

where I is inertia which equals to $\frac{1}{3} ml^2$ and $\dot{q}$ is angular velocity. So the equation of kinetic energy of the link is

$$E_k = \frac{ml^2 \dot{q}^2}{6} \tag{4.2.2}$$

where m is the mass of the link which is 1.265 kg and l is length of the link which is 0.45 m. Also the potential energy of the system is

$$E_p = 0.5 mglcos(q) \tag{4.2.3}$$

where g is gravitational acceleration ($9.81\ m/s^2$). So the L term becomes

$$L = \frac{ml^2 \dot{q}^2}{6} - 0.5 mglcos(q) \tag{4.2.4}$$

Now this L term must be substituted in the equation (4.1.1. So

$$\frac{\mathrm{d}}{\mathrm{dt}}\left(\frac{\partial(\frac{ml^2\dot{q}^2}{6}-0.5mglcos(q))}{\partial\dot{\mathrm{q}}_\mathrm{i}}\right)-\left(\frac{\partial(\frac{ml^2\dot{q}^2}{6}-0.5mglcos(q))}{\partial\mathrm{q}}\right)=\mathrm{Q_i} \qquad (4.2.5)$$

where $\mathrm{Q_i}$ is the torque in this case. So when the $m, l\ and\ g$ values are substituted in equation (4.2.5 and the math is performed, the equation of the motion of this system becomes

$$0.0853875\ddot{q}-2.7921\sin(\mathrm{q})=\tau \qquad (4.2.6)$$

This equation is nonlinear because of the $\sin(\mathrm{q})$ term. In order to simplify the control action, this equation can be linearized via using small angle approximation. Small angle approximation suggests that when the angle approximates to zero the term $\sin(\mathrm{q})$ approximates to q. So the equation becomes

$$0.0853875\ddot{q}-2.7921\mathrm{q}=\tau \qquad (4.2.7)$$

Now the Laplace transformation must be performed to eq. (4.2.7 which gives

$$0.0853875Q(s)s^2-2.7921\mathrm{Q(s)}=\tau(s) \qquad (4.2.8)$$

so the transfer function of the system becomes

$$\frac{Q(s)}{\tau(s)}=\frac{1}{0.0853875s^2-2.7921} \qquad (4.2.9)$$

The standart equation of second order systems was aforementioned ((4.1.15). To be able to make the system's equation similar to the standart second order system equation, an s term must be added to system's equation which is possible via using PD controller. When the PD controller added to the system, the equation becomes

$$s^2-32.7+\frac{k_p}{0.0853875}+\frac{k_d s}{0.0853875}=s^2+2\xi w_n s+{w_n}^2 \qquad (4.2.10)$$

When the ξ and w_n terms are choosen as similar values with the values in CoM control, k_p and k_d constants becomes 11.33 and 1.7, respectively. Figure 4.2.2 depicts the simulink model of the thigh system. The data obtained for the first link (can be seen in Figure 3.2.3.3-a) is given to the system as reference signal. For PD controller, k_p and k_d values which are found above are given as proportional and derivative gains. PD controller parameters can be seen in Figure 4.2.3.

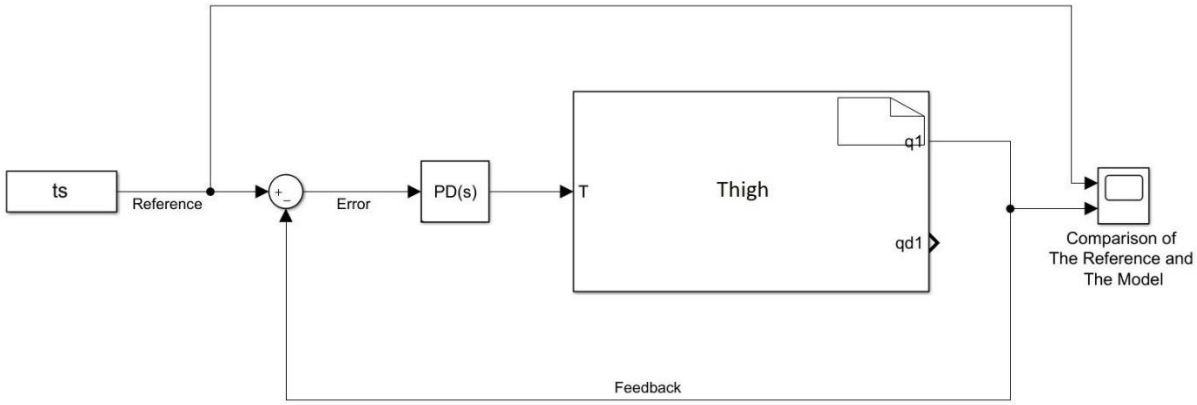

Figure 4.2.2 Simulink model of the thigh

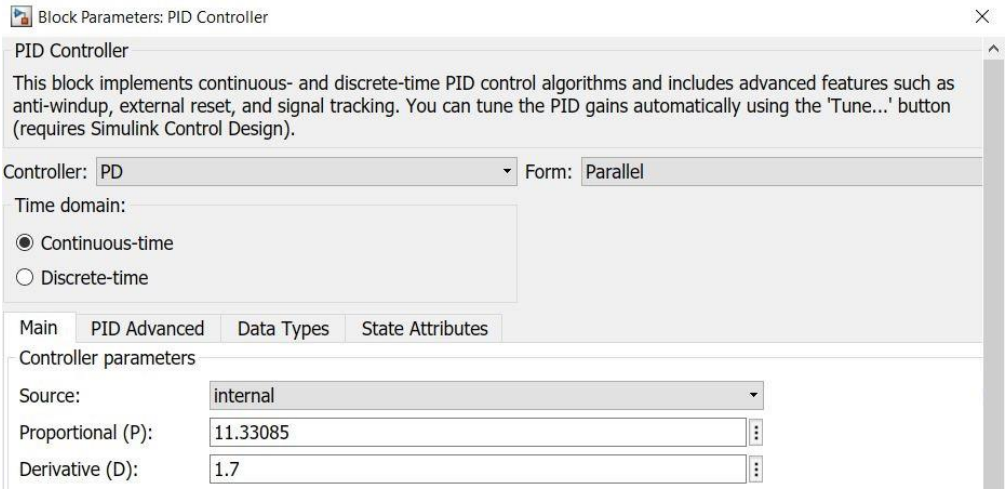

Figure 4.2.3 PD controller parameters for thigh system

The result of the simulation is demonstrated in Figure 4.2.4. Note that the angle of the link follows the desired trajectory but in the beginning of the motion, the angle

goes up to approximately 44.76° (Figure 4.2.5) while the reference signal is nearly 36°. It means that the system has

$$\frac{44.76 - 36}{36} * 100 \approx 25\% \tag{4.2.11}$$

amount of overshoot.

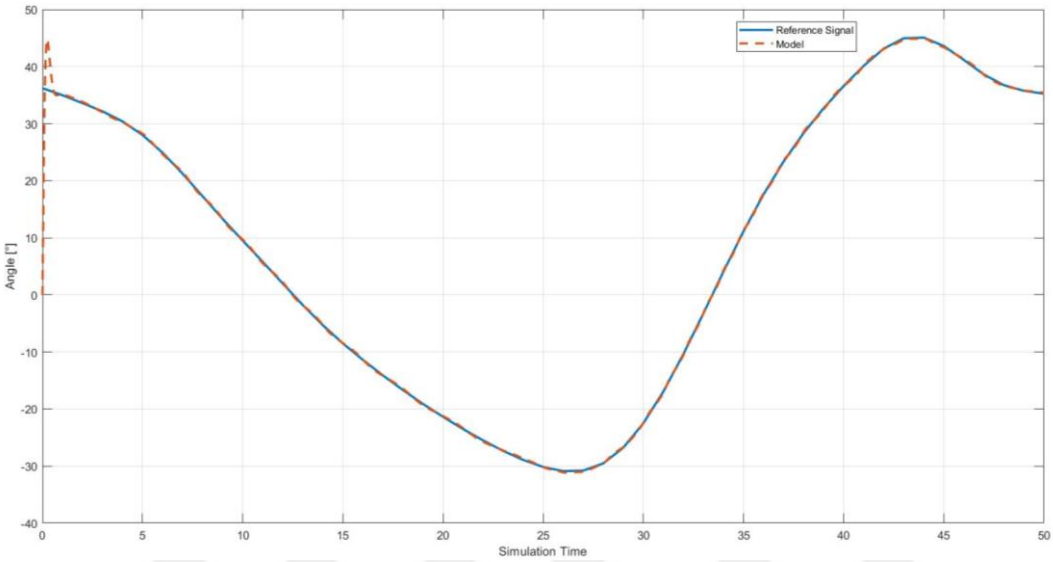

Figure 4.2.4 The result of the simulation

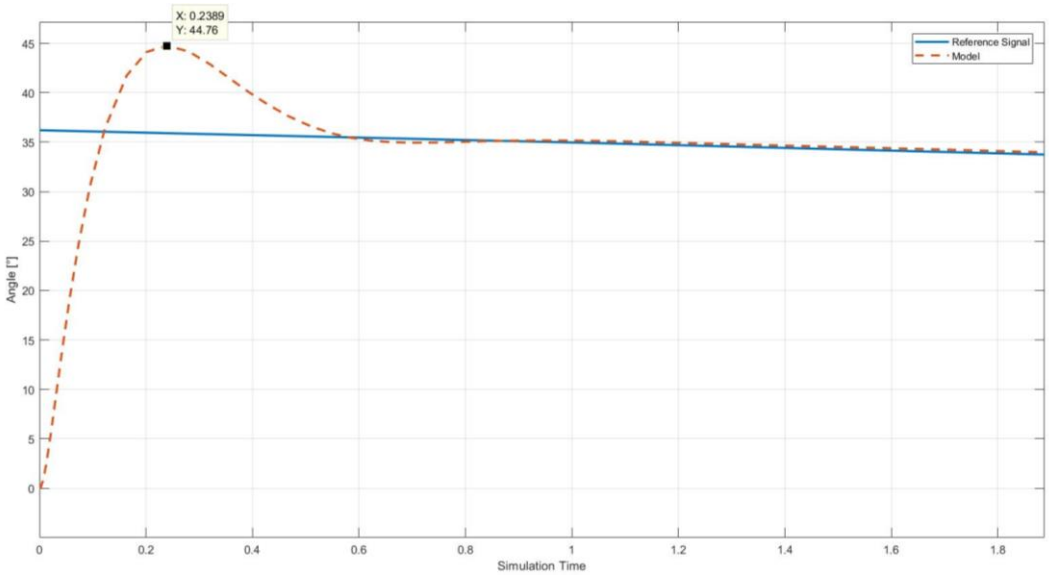

Figure 4.2.5 Overshoot of the model

%25 overshoot is a high value for this system because a slight change in angle can effect the walking negatively. To be able to reduce the overshoot, derivative gain must be tuned. 1.7, 10 and 20 values are used for tuning. Maximum overshoot value is better with the derivative gain of 10. The max. value reaches to approximately 40° which corresponds to

$$\frac{40 - 36}{36} * 100 = 11.1\% \tag{4.2.12}$$

amount of overshoot. When the D gain is set to 20, the maximum overshoot becomes

$$\frac{44 - 36}{36} * 100 = 22.2\% \tag{4.2.13}$$

which is undesirable for this system.

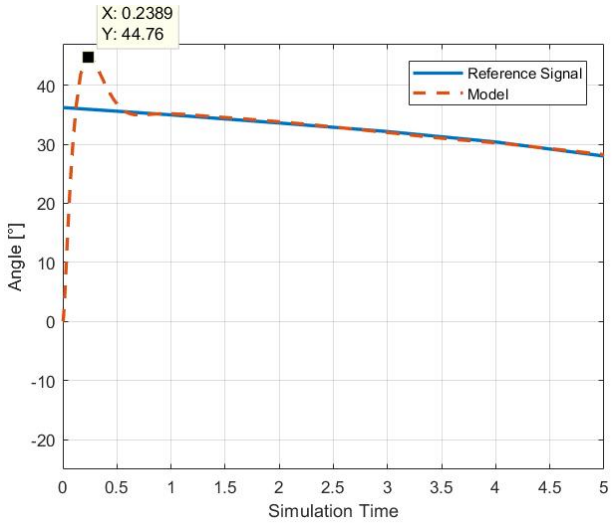

a)

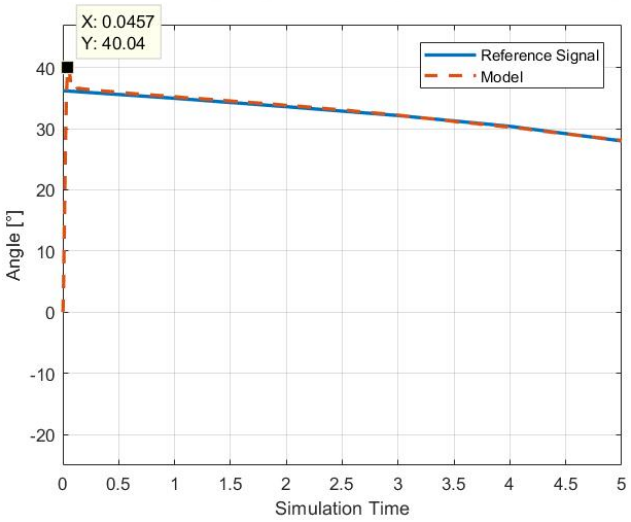

b)

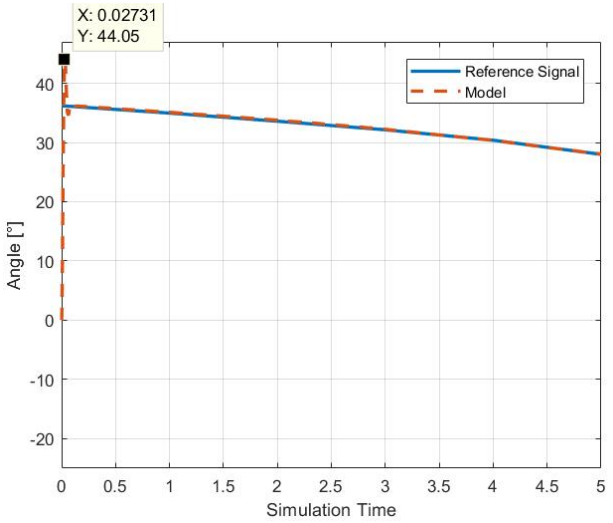

c)

Figure 4.2.6 Comparison of different derivative gains (a)1.7, b)10, c)20)

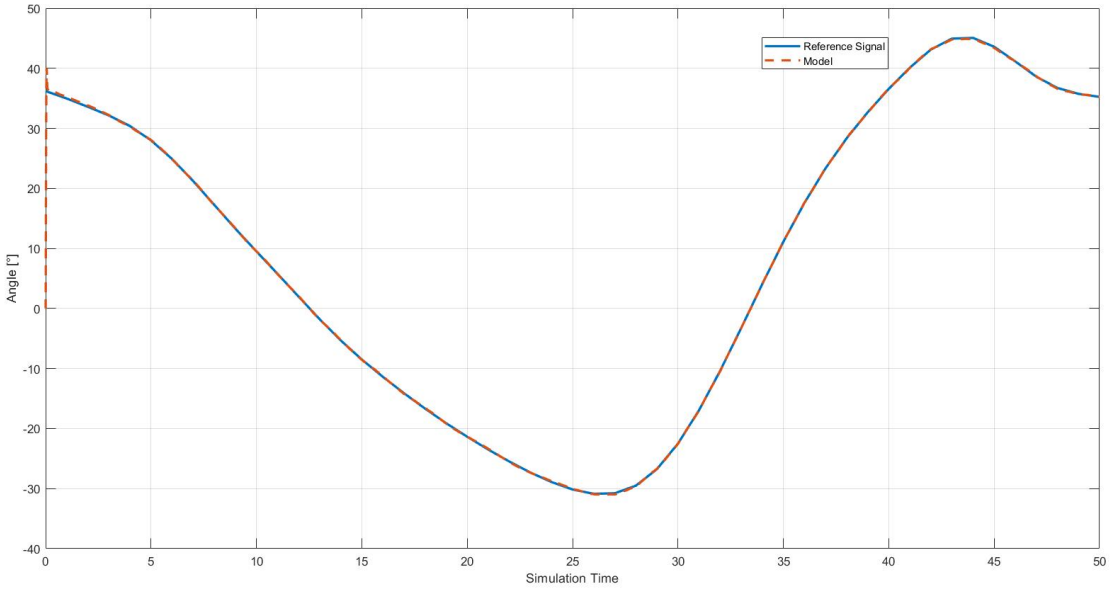

Figure 4.2.7 Final result of the thigh simulation

Chapter 5

Conclusions and Future Prospects

5.1 Conclusions

In this thesis a conceptual design of a knee exoskeleton that assists weight acceptance, sit to stand, push-off, swing and stair ascent motions and a test platform that is built to evaluate lower limb assistive devices are presented. To be able to do this, first, the biomechanical data of these motions were analyzed. Then, considering these data, coefficients of springs that would aid these motions were determined. Results showed that even though there are some differences between the actual data and conceptual design, using elastic elements would be sufficient to assist these motions to achieve energy-efficient devices. Differences are mainly due to non-linear elastic behavior of the natural knee joint, in other words, variable joint stiffness during these motions. However, we apply these motions with linear springs on the exoskeleton, so the exoskeleton joint have constant elastic coefficient. For stair ascent motion, we used an actuator that combines spring and a dc motor with a ball-screw mechanism. Motor is employed to compress the spring, then, together with the spring this actuator assists to raise the body. With this combination the maximum power consumption decreased from nearly 170 W to 130 W in comparison to direct-drive of the knee joint with a dc motor. Currently we are building the prototype of this conceptual design to test the device first functionally and then on individuals to evaluate the performance of the device.

Then, a universal test platform design for lower-limb assistive devices was presented and three conceptual designs for actuating the thigh efficiently were compared. First, a cam design that is meant to build to generate the CoM motion of body was introduced. But some obstacles (discussed in section 3.2.1) showed that using cam in test bed is not effective. Then ballscrew mechanism was proposed. After that three conceptual designs which are direct drive, four-bar mechanism and four-bar with spring mechanism to replicate the thigh link motion were compared. Results showed that when the hip is

actuated by four-bar, the required torque reduced by nearly 66%. There is no difference between the power consumption between direct drive and four-bar mechanism. After the torsional spring is employed on the system however, the power consumption and peak power requirement has been reduced considerably. This would yield a half size of motor for the proposed system compared to the direct-drive system. These results showed that actuating the hip with four-bar with spring mechanism is more feasible and efficient for the design of a test platform. After the conceptual design is defined, PID controller for test platform is performed. To be able to this, first, equations of motion of center of mass and thigh link is obtained by Lagrange Equation. Then PID controller parameters are found and simulations in MATLAB-Simulink are carried out. Simulation results showed that test platform can replicate the desired motion by using PID controller.

5.2 Future Prospects

In this thesis, conceptual design of an exoskeleton that is able to perform weight acceptance, push-off, swing, sit to stance and stair climbing motions and a test platform that can replicate the hip motions which are center of mass motion in vertical direction and hip joint motions are introduced. Simulation results showed that these two designs can mimic the desired motions which are highly important for daily life of individuals.

These conceptual designs are in the process of prototyping. Figure 5.2.1 shows the parts that are processed with CNC router machine. For future prospects, tests of exoskeleton with test bed and individuals that are healthy and unhealthy will be performed after prototypes are built. Improvements of exoskeleton on topology optimization, energy recycling, reducing energy consumption, converging the working principles of joints to real healthy human joints and controlling the exoskeleton with artificial intelligence are planned to studied. Besides, new controller algorithms such as empedance controller, computed torque controller for test platform will be examined.

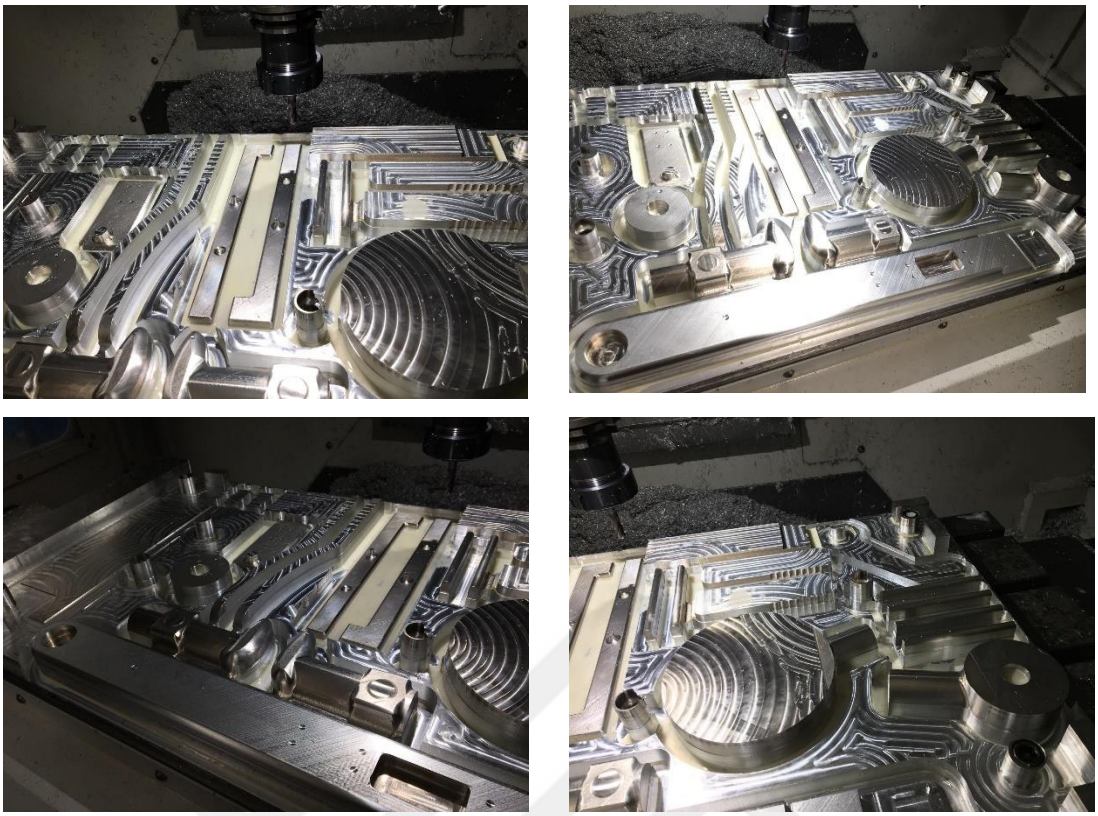

Figure 5.2.1 Parts of conceptual designs

BIBLIOGRAPHY

[1] A. B. Zoss, H. Kazerooni, and A. Chu, “Biomechanical Design of the Berkeley Lower Extremity Exoskeletong (BLEEX),” *IEEE/ASME Trans. Mechatronics*, vol. 11, no. 2, pp. 128–138, 2006.

[2] S. K. Banala, S. K. Agrawal, and J. P. Scholz, “Active Leg Exoskeleton (ALEX) for Gait Rehabilitation of Motor-Impaired Patients,” vol. 0, no. c, 2007.

[3] “Indego – Powering People Forward | Parker Indego.” [Online]. Available: http://www.indego.com/indego/en/home. [Accessed: 02-Nov-2017].

[4] “Rex Bionics - Step into the future.” [Online]. Available: https://www.rexbionics.com/. [Accessed: 02-Nov-2017].

[5] “ReWalk 6.0 – Home.” [Online]. Available: http://rewalk.com/. [Accessed: 02-Nov-2017].

[6] A. P. Exoskeleton, “A Passive Exoskeleton with Artificial Tendons ©,” no. December, pp. 56–61, 2014.

[7] S. K. Agrawal, S. K. Banala, and A. Fattah, “A Gravity Balancing Passive Exoskeleton for the Human Leg,” *Robot. Sci. Syst.* , no. 302, 2006.

[8] “Exoskeleton Technologies: Industrial · Lockheed Martin.” [Online]. Available: https://www.lockheedmartin.com/us/products/exoskeleton/industrial.html. [Accessed: 02-Nov-2017].

[9] “Againer-ski | Maximize your skiing.” [Online]. Available: http://againer-ski.com/?v=ebe021079e5a. [Accessed: 02-Nov-2017].

[10] K. Shamaei, M. Cenciarini, A. A. Adams, K. N. Gregorczyk, J. M. Schiffman, and A. M. Dollar, “Design and evaluation of a quasi-passive knee exoskeleton for investigation of motor adaptation in lower extremity joints,” *IEEE Trans. Biomed. Eng.*, vol. 61, no. 6, pp. 1809–1821, 2014.

[11] A. M. Dollar and H. Herr, “Design of a quasi-passive knee exoskeleton to assist running,” in *2008 IEEE/RSJ International Conference on Intelligent Robots and Systems, IROS*, 2008, pp. 747–754.

[12] H. Van Der Kooij, J. Veneman, and R. Ekkelenkamp, “2006 - van der Kooij et al. - Design of a compliantly actuated exo-skeleton for an impedance controlled gait trainer robot,” pp. 189–193, 2006.

[13] L. J. Junpeng Wu,Jinwu Gao,Rong Song,Rihui Li,Yaning Li, “The design and control of a 3DOF lower limb rehabilitation robot,” in *Mechatronics*, 2016, vol. 33, pp. 13–22.

[14] D. P. Ferris, K. E. Gordon, G. S. Sawicki, and A. Peethambaran, “An improved powered ankle-foot orthosis using proportional myoelectric control,” *Gait Posture*, vol. 23, no. 4, pp. 425–428, 2006.

[15] D. P. Ferris, J. M. Czerniecki, and B. Hannaford, “An ankle-foot orthosis powered by artificial muscles,” *J. Appl. Biomech.*, vol. 21, pp. 189–197, 2005.

[16] L. L. Cai, A. J. Fong, L. Yongqiang, J. Burdick, and V. R. Edgerton, “Assist-as-needed training paradigms for robotic rehabilitation of spinal cord injuries,” in *Proceedings - IEEE International Conference on Robotics and Automation*, 2006, vol. 2006, no. May, pp. 3504–3511.

[17] S. Jezernik, G. Colombo, T. Keller, H. Frueh, and M. Morari, “Robotic Orthosis Lokomat: A Rehabilitation and Research Tool,” *Neuromodulation*, vol. 6, no. 2, pp. 108–115, 2003.

[18] Xiaopeng Liu and K. H. Low, “Development and preliminary study of the NTU lower extremity exoskeleton,” in *IEEE Conference on Cybernetics and Intelligent Systems, 2004.*, 2004, vol. 2, pp. 1243–1247.

[19] H. Kazerooni, R. Steger, and L. Huang, “Hybrid Control of the Berkeley Lower Extremity Exoskeleton (BLEEX),” *Int. J. Rob. Res.*, vol. 25, no. 5–6, pp. 561–573, 2006.

[20] H. Richter, D. Simon, W. A. Smith, and S. Samorezov, “Dynamic modeling, parameter estimation and control of a leg prosthesis test robot,” *Appl. Math. Model.*, vol. 39, no. 2, pp. 559–573, 2015.

[21] O. Jones, “Anatomical Planes - Coronal - Sagittal - TeachMeAnatomy.” 2017.

[22] D. E. Lunn, A. Lampropoulos, and T. D. Stewart, “Basic biomechanics of the hip,” *Orthop. Trauma*, vol. 30, no. 3, pp. 239–246, 2016.

[23] R. Shenoy, P. S. Pastides, and D. Nathwani, "(iii) Biomechanics of the knee and TKR," *Orthop. Trauma*, vol. 27, no. 6, pp. 364–371, 2013.

[24] C. L. Brockett and G. J. Chapman, "Biomechanics of the ankle," *Orthop. Trauma*, vol. 30, no. 3, pp. 232–238, 2016.

[25] R. Baxter, N. Hastings, A. Law, and E. J. . Glass, *Basic Biomechanics of the MUSCULOSKELETAL SYSTEM*, vol. 39, no. 5. 2008.

[26] D. A. Winter, *The Biomechanics and Motor Control of Human Gait*. 1991.

[27] J. Merker, M. Hartmann, F. Kreuzpointner, A. Schwirtz, and J. P. Haas, "Pathophysiology of juvenile idiopathic arthritis induced pes planovalgus in static and walking condition-A functional view using 3d gait analysis," *Pediatr. Rheumatol.*, vol. 13, no. 1, pp. 1–11, 2015.

[28] "8 phases of human gait cycle." [Online]. Available: https://www.streifeneder.com/downloads/o.p./400w43_e_poster_gangphasen_druck.pdf.

[29] "Human Skeletal Muscles Explained - Origin, insertion, joint actions." [Online]. Available: http://www.sportsinjuryclinic.net/anatomy/human-muscles. [Accessed: 12-Dec-2017].

[30] M. J. McAllister, K. G. Hammond, B. K. Schilling, L. C. Ferreria, J. P. Reed, and L. W. Weiss, "Muscle Activation During Various Hamstring Exercises," *J. Strength Cond. Res.*, vol. 28, no. 6, pp. 1573–1580, Jun. 2014.

[31] "E is for the 'Erector Spinae' | Future Fit Training." [Online]. Available: https://www.futurefit.co.uk/pilates/resources/a-z/2015/01/15/e-is-for-the-erector-spinae/. [Accessed: 12-Dec-2017].

[32] "The Definitive Guide to Gastrocnemius Anatomy, Exercises & Rehab." [Online]. Available: http://www.kingofthegym.com/gastrocnemius/. [Accessed: 12-Dec-2017].

[33] "Peroneal Tendonitis (Tendinopathy) - Rehab4Runners." [Online]. Available: http://www.rehab4runners.co.uk/running-injuries/lower-leg-pain/peroneal-tendonitis-tendinopathy/. [Accessed: 12-Dec-2017].

[34] R. Riener, M. Rabuffetti, and C. Frigo, “Stair ascent and descent at different inclinations,” *Gait Posture*, vol. 15, no. 1, pp. 32–44, 2002.

[35] J. Sandra, “Predicting step time from step length and velocity,” *Aust. J. Physiother.*, vol. 38, no. 1, pp. 43–46.

[36] M. S. Orendurff, A. D. Segal, G. K. Klute, J. S. Berge, E. S. Rohr, and N. J. Kadel, “The effect of walking speed on center of mass displacement,” *J. Rehabil. Res. Dev.*, vol. 41, no. 6, p. 829, 2004.

[37] M. A. F. Sanjuán, *An Introduction to Lagrangian Mechanics, by A.J. Brizard*, vol. 51, no. 5. 2010.

[38] A. E.-N. Gene F. Franklin, J. David Powell, *Feedback Control of Dynamic Systems*. Addison-Wesley, 1993.

[39] N. S. Nise, “Control System Engineering.” Wiley, 2004.

[40] K. Ogata, *Modern Control Engineering*. Prentice Hall, 2010.

[41] J. K. Budynas, Richard G., Nisbett, *Shigley’s Mechanical Engineering Design*. Mc Graw Hill, 2011.

[42] R. C. Hibbeler, *Engineering Mechanics: Dynamics*. Pearson, 2010.

APPENDIX

3.1.1 Weight Acceptance Spring

```
clear all
clc
close all

q = [ 3.97 7 10.52 14.12 17.38 19.84 21.27 21.67 21.22 20.20 18.86
17.35 15.73 14.08 12.50 11.09 9.91 8.97 8.28 7.86 7.72 7.94 8.6 9.76
11.50 13.86 16.97 20.96 26 32.03 38.74 45.6 52.05 57.54 61.66 64.12
64.86 63.95 61.59 57.97 53.27 47.58 40.94 33.46 25.38 17.27 9.94 4.31
1.12 0.54 2.21];
T_kn = 80*[-0.196 -0.281 -0.090 0.173 0.362 0.508 0.593 0.615 0.556
0.469 0.362 0.244 0.141 0.052 -0.019 -0.070 -0.114 -0.149 -0.181 -
0.217 -0.247 -0.237 -0.171 -0.087 -0.004 0.054 0.116 0.157 0.156 0.114
0.080 0.066 0.064 0.053 0.037 0.020 0.004 -0.009 -0.023 -0.040 -0.059
-0.082 -0.114 -0.158 -0.211 -0.253 -0.263 -0.224 -0.147];

l1=78;
l2=150;
l3=67.5;
Ox=0;
Oy=0;
k=14500;

for i=1:51
    Bx(i)=l3;
    By(i)=-(((l2^2)-(Ax(i)+l3)^2)^0.5)+Ay(i);
    l4(i)=(Bx(i)^2+By(i)^2)^0.5;
    theta(i)=acosd((l1^2+l2^2-l4(i)^2)/(2*l1*l2));
    f(i)=(T_kn(i)*1000)/(l1*sind(theta(i)));
    beta(i)=asind((l3-Ax(i))/l2);
    fyay(i)=f(i)*cosd(beta(i));
    uzama_metre(i)=uzama(i)/1000;

torkyay(i)=k*uzama_metre(i)*(1/cosd(beta(i)))*(l1/1000)*sind(theta(i))
;

end
data=0:2:100;

subplot(3,1,1)
plot(q)
subplot(3,1,2)
plot(By)
subplot(3,1,3)
plot(uzama)

figure
plot(uzama_metre,fyay)
grid on
ylabel('Force [N]')
xlabel('Elongation [m]')

figure
```

```
plot(data(2:17),T_kn(2:17))
hold on
plot(data(2:17),torkyay(2:17))
grid on
ylabel('Moment [Nm]')
xlabel('% of cycle')
legend('Actual Knee' ,'Spring')
```

3.1.2 Sit to Stance Spring

```
clear all
clc
close all

lt=0.45;
l1=154;
Bx=-36;
By=-129.5;
l2=134.41/1000;
s0=65/1000;
k1=14500;

for i=1:90
    knee_angle(i)=i-1;
    T(i)=50*9.81*lt*cosd(90-knee_angle(i));
    Ax(i)=l1*cosd(270-41-knee_angle(i));
    Ay(i)=l1*sind(270-41-knee_angle(i));
    xx(i)=-atand((Ay(i)-By)/(Ax(i)-Bx));
    zz(i)=180-xx(i)-74.46;
    lever_arm(i)=l2*sind(zz(i));
    force(i)=T(i)/lever_arm(i);
    yay(i)=(((Ay(i)-By)^2+(Ax(i)-Bx)^2)^0.5)/1000;
    uzama(i)=yay(i)-s0;
    yaytork(i)=k1*uzama(i)*lever_arm(i);


end

plot(uzama,force)
grid on
ylabel('Force [N]')
xlabel('Elongation [m]')

figure
plot(T)
hold on
plot(yaytork)
grid on
ylabel('Moment [N.m]')
xlabel('Angle of Knee [deg]')
legend('Knee Moment','Spring Moment')
```

3.1.3 Stair Ascent Spring

```
clear all
clc
close all

q=[0 76.8560688527425 76.5103330265045 76.2434314637984
76.0038788515326 75.7163103122657 75.2964422060175 74.6851542165428
73.8632444496476 72.8439199868454 71.6550322496239 70.3224703846294
68.8645634082937 67.2865047247271 65.5967773799710 63.8132995050211
61.9493760078540 60.0029576540195 57.9898069440036 55.9119980973897
53.7716800717896 51.5788951449065 49.3401594795255 47.0642110179892
44.7651766275460 42.4535481443091 40.1414887745331 37.8436526852631
35.5716854883118 33.3388659729582 31.1498742755016 29.0428452673533
27.0197256118677 25.0903249565101 23.2568930590343 21.5242603366938
19.8936238144177 18.4103450391650 17.0650369388882 15.8658134407322
14.8102418246663  11.9029001768763 11.4371080102995 11.0489877122809
10.7363159910716 10.4837222815472 10.3095777755260 10.1727839730787
10.0426719143365 9.93530720224487 9.85741382889726 9.79954549830231
9.78077327456501 9.83564857988285 10.0008478661255 10.3332700422702
10.8977563154629 11.7640573639283 13.0154737067220 14.7342592580894
17.0254353303519 19.9004550927020 23.4083590773504 27.5306156036847
32.2108449472097 37.3544615855692 42.8398958419532 48.5312183735261
54.2919058269782 60.0010046303475 65.5616362177265 70.8981433483483
75.9510251904270 80.6730474064667 85.0203757787668 88.9518972636519
92.4328277948241 95.4312567868602 97.9175412976758 99.8720015880314
101.283991622480 102.154590451313 102.497953700330 102.342055086519
101.728660532879 100.710574573158 99.3484833199053 97.7094447063919
95.8670108623895 93.9005590722971 91.8906166859618 89.9111864040347
88.0229306517364 86.2718335906374 84.6956682905961 83.3316275736362
82.2099887349546 81.3351449712118];
T_kn=80*[0 -0.0575788517538208 -0.0372375883507033 -
0.00817929192586367 0.0353163000844085 0.0972243195434552
0.177304191838217 0.271675766120301 0.374877922305645
0.482500851091904 0.591549071571235 0.699237037778282
0.801631330063952 0.893889864131788 0.971630833087017 1.03190805639295
1.07326166529375 1.09532565339531 1.09852057305738 1.08398067785623
0.679633342068793 0.609573042983496 0.542806861579621
0.480530734219078 0.423341502436305 0.371380369342036
0.324499530629443 0.282374884286969 0.244485499683962
0.210044941396656 0.178177402669937 0.148155243104304
0.119650483392854 0.0926084950104522 0.0669971546916579
0.0426085999610643 0.0189884198985942 -0.00441642009254467 -
0.0282043649273693 -0.0528421471278713 -0.0784780306338790 -
0.104803828093113 -0.131089489174975 -0.156262815576996 -
0.178986111881762 -0.197746141457654 -0.211017651291695 -
0.217645508713685 -0.217022564802837 -0.209458447722903 -
0.196124551680068 -0.178813178546337 -0.159564883511725 -
0.140428622233351 -0.123451748641186 -0.110495797486514 -
0.102863284429095 -0.100785224751758 -0.103316056093910 -
0.108298291240797 -0.113066465807123 -0.114971721686189 -
0.112125934536625 -0.103711385446054 -0.0901240398334636 -
0.0726895971305885 -0.0531869755243455 -0.0333895861387258 -
0.0147660788178206 0.00164537253515318 0.0152216030500434
0.0256748338954806 0.0329390025007115 0.0370498125289276
0.0380768003045873 0.0360982579441120 0.0311991330168428
0.0234527697801640 0.0129108474293907 -0.000408124020445063 -
0.0164488963632642 -0.0350234808985586 -0.0557088134258555 -
0.0777978922029720 -0.100305200763154 -0.122021772306264 -
0.141601946874271 -0.157784598911273 -0.169528361744056 -
```

```
0.175882635041288 -0.175205088808617 -0.164789878807619 -
0.142772928925807 -0.110592763582282 -0.0719815126214015];

k=14500;
l1=78;
l2=150;
l3=67.5;
Ox=0;
Oy=0;

for i=1:101
    Bx(i)=l3;
    By(i)=-(((l2^2)-(Ax(i)+l3)^2)^0.5)+Ay(i);
    l4(i)=(Bx(i)^2+By(i)^2)^0.5;
    theta(i)=acosd((l1^2+l2^2-l4(i)^2)/(2*l1*l2));
    f(i)=(T_kn(i)*1000)/(l1*sind(theta(i)));
    beta(i)=asind((l3-Ax(i))/l2);
    fyay(i)=f(i)*cosd(beta(i));
    uzama_metre(i)=uzama(i)/1000;


torkyay(i)=k*uzama_metre(i)*(1/cosd(beta(i)))*(l1/1000)*sind(theta(i))
;
    torkmotor(i)=torkyay(i)-T_kn(i);
    f_m(i)=f(i)-uzama_metre(i)*k;
    actuator_torque(i)=torkyay(i)-T_kn(i);

end

subplot(3,1,1)
plot(q)
subplot(3,1,2)
plot(By)
subplot(3,1,3)
plot(uzama)

figure
plot(uzama_metre,fyay)

figure
plot(T_kn)
hold on
plot(torkyay)
grid on
ylabel('Moment [Nm]')
xlabel('% of cycle')
legend('Actual Knee','Spring')

figure
plot(actuator_torque)
grid on
```

3.1.4 Swing and Push-Off Spring

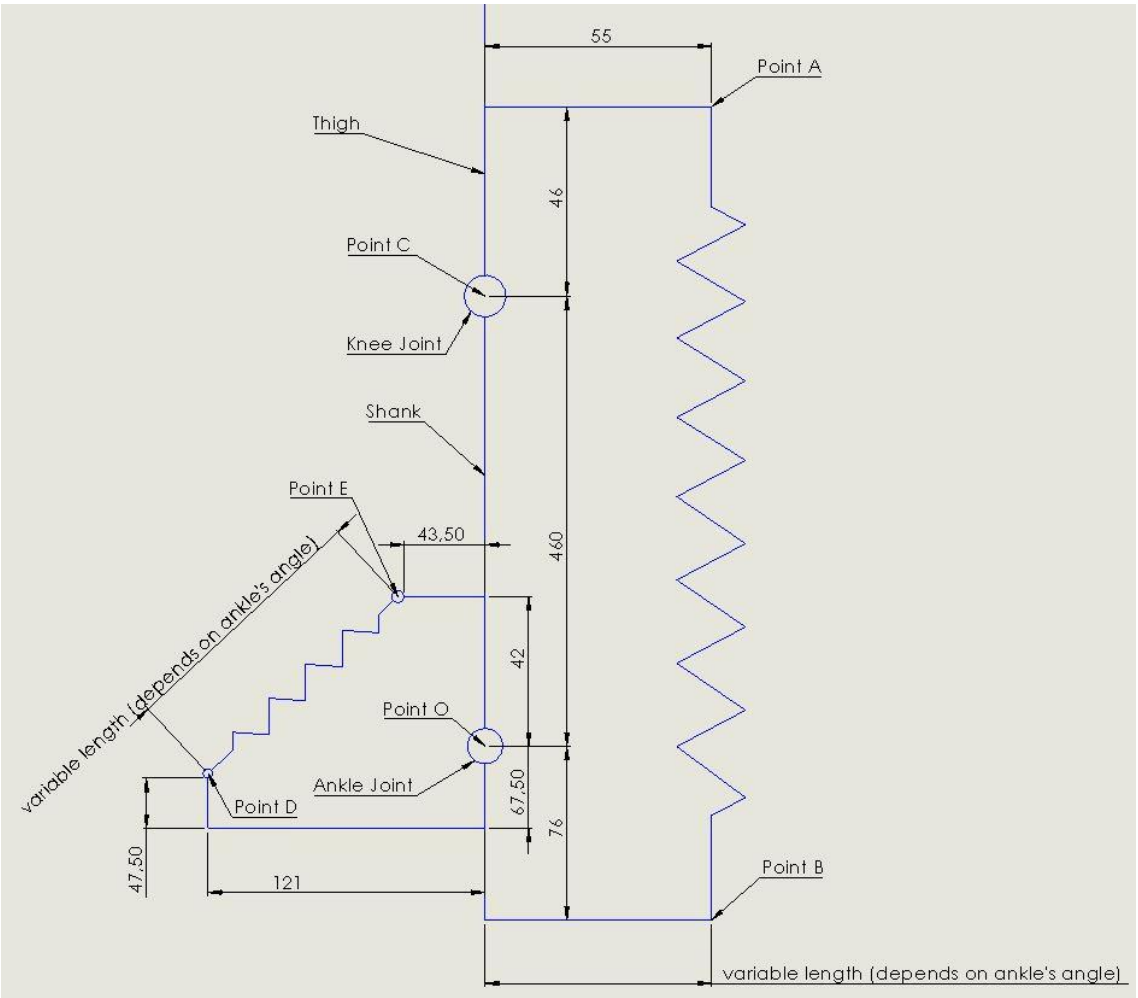


```
clear all
close all
clc

% Human Joint Torque data during Normal Walking
m = 75;
t=0:50;
T_hn = m*[0 0.249 0.600 0.556 0.416 0.359 0.305 0.245 0.159 0.084 0 -
0.064 -0.092 -0.098 -0.092 -0.085 -0.088 -0.1 -0.130 -0.168 -0.199 -
0.231 -0.269 -0.312 -0.364 -0.401 -0.404 -0.356 -0.262 -0.251 -0.310 -
0.344 -0.295 -0.228 -0.169 -0.126 -0.089 -0.069 -0.057 -0.044 -0.026 -
0.009 0.008 0.029  0.242 0.296 0.301 0.237 0.118];
T_kn = m*[0 -0.196 -0.281 -0.090 0.173 0.362 0.508 0.593 0.615 0.556
0.469 0.362 0.244 0.141 0.052 -0.019 -0.070 -0.114 -0.149 -0.181 -
0.217 -0.247 -0.269 -0.270 -0.237 -0.171 -0.087 -0.004 0.054 0.116
0.157 0.156 0.114 0.080 0.066 0.064 0.053 0.037 0.020 0.004 -0.009 -
0.023 -0.040 -0.059 -0.082 -0.114 -0.158 -0.211 -0.253 -0.263 -0.224 -
0.147];
T_an = m*[0 -0.009 -0.034 -0.064 -0.051 0.028 0.143 0.260 0.368 0.469
0.545 0.601 0.650 0.692 0.736 0.780 0.825 0.881 0.951 1.037 1.144
1.260 1.388 1.513 1.608 1.628 1.565 1.388 1.073 0.690 0.335 0.102 -
0.001 -0.028 -0.023 -0.010 -0.011 -0.012 -0.013 -0.013 -0.011 -0.006
0.001 0.007 0.011 0.010 0.004];
```

```
Theta_hip_n = [0 19.33 18.92 18.45 17.94 17.30 16.40 15.18 13.67 11.97
10.21 8.48 6.74 4.94 3.13 1.42 -0.13 -1.54 -2.87 -4.12 -5.30 -6.40 -
7.43 -8.39 -9.27 -10.02 -10.61 -10.95 -10.91 -10.31 -9.00 -6.95 -4.25
-1.05 2.42 5.93 9.22 12.11 14.55 16.53 18.13 19.45 20.54 21.38 21.84
21.87 21.50 20.84 20.09 19.50 19.18 19.01];
Theta_knee_n = [0 3.97 7 10.52 14.12 17.38 19.84 21.27 21.67 21.22
20.20 18.86 17.35 15.73 14.08 12.50 11.09 9.91 8.97 8.28 7.86 7.72
7.94 8.6 9.76 11.50 13.86 16.97 20.96 26 32.03 38.74 45.6 52.05 57.54
61.66 64.12 64.86 63.95 61.59 57.97 53.27 47.58 40.94 33.46 25.38
17.27 9.94 4.31 1.12 0.54 2.21];
Theta_ankle_n = [0 0.02 -2.06 -3.88 -4.6 -3.98 -2.40 -0.45 1.45 3.04
4.27 5.13 5.71 6.10 6.43 6.76 7.12 7.54 7.99 8.44 8.86 9.23 9.51 9.62
9.43 8.70 7.20 4.69 1.15 -3.26 -8.17 -13.05 -17.13 -19.52 -19.77 -
18.12 -15.29 -12.04 -8.85 -5.96 -3.51 -1.64 -0.50 -0.07 -0.16 -0.42 -
0.52 -0.26 0.36 1.00 1.20 0.58];
ls1=500;
Cx=0;
Cy=460;
k_sw=5064;

%swing=============================================================
for i=1:52;
    Ax(i)=71.7*cosd(40-Theta_knee_n(i));
    Ay(i)=71.7*sind(40-Theta_knee_n(i))+460;
    la(i)=78+1.46*Theta_ankle_n(i);
    Q1(i)=atand(la(i)/76);
    lb(i)=(la(i)^2+76^2)^0.5;
    Bx(i)=lb(i)*cosd(270+Q1(i)-Theta_ankle_n(i));
    By(i)=lb(i)*sind(270+Q1(i)-Theta_ankle_n(i));
    l1(i)=((Ax(i)-Bx(i))^2+(Ay(i)-By(i))^2)^0.5;
    elong1(i)=(ls1-l1(i))/1000;
    Q2(i)=acosd((71.7^2+l1(i)^2-(Bx(i)-Cx)^2-(By(i)-
Cy)^2)/(2*71.7*l1(i)));
    f1(i)=(1000*T_kn(i))/(55*sind(40+Q2(i)));
    T_sw(i)=k_sw*elong1(i)*0.055*sind(40+Q2(i));
end

plot(elong1)

figure
plot(f1)

figure
plot(elong1,f1)
grid on
ylabel('Force [N]')
xlabel('Elongation [m]')

figure
plot(T_sw)
hold on
plot(T_kn)
grid on



%push-off==========================================================
Ex=-43.6;
Ey=42;
ls2=110;
k_po=134000;
```

```
for i=1:52
    Dx(i)=122.6*cosd(190-Theta_ankle_n(i));
    Dy(i)=122.6*sind(190-Theta_ankle_n(i));
    l2(i)=((Dx(i)-Ex)^2+(Dy(i)-Ey)^2)^0.5;
    elong2(i)=(ls2-l2(i))/1000;
    Q3(i)=acosd((l2(i)^2+62^2-47.5^2)/(124*l2(i)));
    f2(i)=((T_an(i)-T_sw(i))*1000)/(43.6*sind(90+Q3(i)));
    T_po(i)=k_po*elong2(i)*0.043*sind(90+Q3(i));
end

figure
plot(elong2,f2)
grid on
ylabel('Force [N]')
xlabel('Elongation [m]')

figure
plot(T_an)
hold on
plot(T_po)
grid on
```

3.2.3 Design

Autolev Codes

```
Frames A,B,C,N
Variables qm, qc, q
Constants l0,l1,l2,l3

Simprot(N,A,3,qm)
Simprot(N,B,3,qc)
Simprot(N,C,3,q)


R>=l0*n1>+l3*c1>
A>=l1*a1>
B>=l2*b1>

LDelta=(Mag(R>)^2+Mag(B>)^2-Mag(A>)^2)/(2*Mag(R>))
URn>=Cross(unitvec(R>),N3>)
Anew>=((Mag(B>)^2-LDelta^2)^0.5)*URn>-((LDelta-Mag(R>))*Unitvec(R>))
Explicit(Anew>)
a2=dot(Anew>,n2>)
a1=dot(Anew>,n1>)
```

Result of the Autolev Codes:

```
a2 = 0.5*l3*SIN(q)*(2+(l1^2-l0^2-l2^2-l3^2-
2*l0*l3*COS(q))/(l0^2+l3^2+2*l0*l3*COS(q))) - (l0+l3*COS(q))*(l2^2-
0.25*(l1^2-l0^2-l2^2-l3^2-
2*l0*l3*COS(q))^2/(l0^2+l3^2+2*l0*l3*COS(q)))^0.5/(l0^2+l3^2+2*l0*l3*C
OS(q))^0.5

a1 = 0.5*l3*COS(q)*(2+(l1^2-l2^2-l3^2-
2*l0*l3*COS(q))/(l0^2+l3^2+2*l0*l3*COS(q))) + 0.5*l0*(2+(l1^2-l0^2-
l2^2-l3^2-3*l0*l3*COS(q))/(l0^2+l3^2+2*l0*l3*COS(q))) +
l3*SIN(q)*(l2^2-0.25*(l1^2-l0^2-l2^2-l3^2-
2*l0*l3*COS(q))^2/(l0^2+l3^2+2*l0*l3*COS(q)))^0.5/(l0^2+l3^2+2*l0*l3*C
OS(q))^0.5
```

MATLAB Codes

```
%Angle of four-bar actuator

clear all
clc
close all

l0=200;
l1=70;
l2=225;
l3=150;
q=(270+[19.3300000000000 18.9200000000000 18.4500000000000
17.9400000000000 17.3000000000000 16.4000000000000 15.1800000000000
13.6700000000000 11.9700000000000 10.2100000000000 8.48000000000000
6.74000000000000 4.94000000000000 3.13000000000000 1.42000000000000 -
0.130000000000000 -1.54000000000000 -2.87000000000000 -
4.12000000000000 -5.30000000000000 -6.40000000000000 -7.43000000000000
-8.39000000000000 -9.27000000000000 -10.0200000000000 -
10.6100000000000 -10.9500000000000 -10.9100000000000 -10.3100000000000
-9 -6.95000000000000 -4.25000000000000 -1.05000000000000
2.42000000000000 5.93000000000000 9.22000000000000 12.1100000000000
14.5500000000000 16.5300000000000 18.1300000000000 19.4500000000000
20.5400000000000 21.3800000000000 21.8400000000000 21.8700000000000
21.5000000000000 20.8400000000000 20.0900000000000 19.5000000000000
19.1800000000000 19.0100000000000]);
Ox=0;
Oy=0;

for i=1:51
a2(i) = 0.5*l3*sind(q(i))*(2+(l1^2-l0^2-l2^2-l3^2-
2*l0*l3*cosd(q(i)))/(l0^2+l3^2+2*l0*l3*cosd(q(i)))) -
(l0+l3*cosd(q(i)))*(l2^2-0.25*(l1^2-l0^2-l2^2-l3^2-
2*l0*l3*cosd(q(i)))^2/(l0^2+l3^2+2*l0*l3*cosd(q(i))))^0.5/(l0^2+l3^2+2
*l0*l3*cosd(q(i)))^0.5;

a1(i) = 0.5*l3*cosd(q(i))*(2+(l1^2-l2^2-l3^2-
2*l0*l3*cosd(q(i)))/(l0^2+l3^2+2*l0*l3*cosd(q(i)))) + 0.5*l0*(2+(l1^2-
l0^2-l2^2-l3^2-3*l0*l3*cosd(q(i)))/(l0^2+l3^2+2*l0*l3*cosd(q(i)))) +
l3*sind(q(i))*(l2^2-0.25*(l1^2-l0^2-l2^2-l3^2-
2*l0*l3*cosd(q(i)))^2/(l0^2+l3^2+2*l0*l3*cosd(q(i))))^0.5/(l0^2+l3^2+2
*l0*l3*cosd(q(i)))^0.5;
```

```
qm(i)=atan2(a2(i),a1(i))*57.2958;

A=line([Ox l1*cosd(qm(i))],[Oy l1*sind(qm(i))])
B=line([l1*cosd(qm(i)) l0+l3*cosd(q(i))],[l1*sind(qm(i))
l3*sind(q(i))])
C=line([l0 l0+l3*cosd(q(i))],[Oy l3*sind(q(i))])

xlim([-50 350])
ylim([-150 0])
grid on

B_length(i)=((l1*cosd(qm(i))-l0-l3*cosd(q(i)))^2+(l1*sind(qm(i))-
l3*sind(q(i)))^2)^0.5;

B_x(i)=l1*cosd(qm(i))-l0-l3*cosd(q(i));
B_y(i)=l1*sind(qm(i))-l3*sind(q(i));

qc(i)=atan2(B_y(i),B_x(i))*57.2958+180;

pause(0.1)
if i<51
    delete(A)
    delete(B)
    delete(C)

end
end

clear all
close all
clc

%Torque comparison between direct drive and four-bar
hip_T=-[-18.6750000000000 -45 -41.7000000000000 -31.2000000000000 -
26.9250000000000 -22.8750000000000 -18.3750000000000 -11.9250000000000
-6.30000000000000 0 4.80000000000000 6.90000000000000 7.35000000000000
6.90000000000000 6.37500000000000 6.60000000000000 7.50000000000000
9.75000000000000 12.6000000000000 14.9250000000000 17.3250000000000
20.1750000000000 23.4000000000000 27.3000000000000 30.0750000000000
30.3000000000000 26.7000000000000 19.6500000000000 18.8250000000000
23.2500000000000 25.8000000000000 22.1250000000000 17.1000000000000
12.6750000000000 9.45000000000000 6.67500000000000 5.17500000000000
4.27500000000000 3.30000000000000 1.95000000000000 0.675000000000000 -
0.600000000000000 -2.17500000000000 -4.50000000000000 -
7.95000000000000 -12.7500000000000 -18.1500000000000 -22.2000000000000
-22.5750000000000 -17.7750000000000 -8.85000000000000];
q=([19.3300000000000 18.9200000000000 18.4500000000000
17.9400000000000 17.3000000000000 16.4000000000000 15.1800000000000
13.6700000000000 11.9700000000000 10.2100000000000 8.48000000000000
6.74000000000000 4.94000000000000 3.13000000000000 1.42000000000000 -
0.130000000000000 -1.54000000000000 -2.87000000000000 -
4.12000000000000 -5.30000000000000 -6.40000000000000 -7.43000000000000
-8.39000000000000 -9.27000000000000 -10.0200000000000 -
10.6100000000000 -10.9500000000000 -10.9100000000000 -10.3100000000000
-9 -6.95000000000000 -4.25000000000000 -1.05000000000000
2.42000000000000 5.93000000000000 9.22000000000000 12.1100000000000
14.5500000000000 16.5300000000000 18.1300000000000 19.4500000000000
20.5400000000000 21.3800000000000 21.8400000000000 21.8700000000000
21.5000000000000 20.8400000000000 20.0900000000000 19.5000000000000
19.1800000000000 19.0100000000000]);
```

```
qm=90+[-53.7921233927568 -55.0290386622894 -56.4048032728825 -
57.8532749319212 -59.6146391474926 -62.0022485093538 -65.1036959579336
-68.7745681247127 -72.7386807466146 -76.7010582398725 -
80.4898381716141 -84.2201526610138 -88.0154019940125 -91.7840866947076
-95.3141642773158 -98.4977888978179 -101.386923918568 -
104.110854986197 -106.673556908534 -109.098134381368 -111.365533872570
-113.496990757611 -115.492547395942 -117.330756911170 -
118.905120531074 -120.149147528007 -120.868424077156 -120.783709537502
-119.515954600063 -116.765773530656 -112.502562341759 -
106.940361907671 -100.383301218151 -93.2526920207034 -85.9349159546475
-78.8802743926026 -72.4178407183085 -66.6551716224105 -
61.6631271533021 -57.3186515096365 -53.4228977109551 -49.8877019198057
-46.8666775123600 -45.0527910858414 -44.9294740435884 -
46.4063805123774 -48.8447759495839 -51.3906590279546 -53.2680277704205
-54.2489396168961 -54.7606288232532];
qc=[337.786731592049 337.931828334625 338.083577715614
338.232692363228 338.399759659876 338.602192176932 338.825817463001
339.036404090610 339.202214327668 339.308213939628 339.357126393877
339.357931517761 339.312864791537 339.224275437256 339.103125419948
338.963147054927 338.811489991385 338.647432433815 338.474677552979
338.294987001556 338.112774419439 337.929079580946 337.746252637105
337.568595197817 337.409406271252 337.279037521156 337.201816960177
337.210981944763 337.345898508097 337.624141410453 338.016274122764
338.455674734271 338.866799150861 339.178287188756 339.343174763162
339.342417849720 339.191071218436 338.921764688795 338.575081905096
338.178906914829 337.741795668245 337.272329490320 336.811968208499
336.507734218452 336.486265778429 336.736791113419 337.119770761490
337.480748895636 337.722722450480 337.841288567304 337.901047440927];
t=1:51;
qdot=diff(q)./diff(t);
qdot=[qdot(1) qdot]/57.2958;
qmdot=diff(qm)./diff(t);
qmdot=[qmdot(1) qmdot]/57.2958;
k=1.2157;

l1=0.070;
l2=0.225;
l3=0.15;

for i=1:51
    force(i)=hip_T(i)/(l3*sind(450-qc(i)+q(i)));
    fourbar_tork(i)=force(i)*l1*sind(450+qm(i)-qc(i));
    power_hip(i)=hip_T(i)*qdot(i);
    power_fourbar(i)=fourbar_tork(i)*qmdot(i);
end
figure
plot(hip_T)
hold on
plot(fourbar_tork)
grid on
figure
plot(power_hip)
hold on
plot(power_fourbar)
grid on
figure
plot(q,hip_T)
grid on
figure
plot(q)
hold on
```

```
plot(qm)
ylabel('Angle [deg]')
legend('Hip Angle','Fourbar Motor Angle')
grid on
close all
clear all
clc


%Power comparison between direct drive, four-bar without spring and
four-bar with spring
hip_power=[-0.133635449718826 -0.322013131852594 -0.342066957787484 -
0.277716691275799 -0.300755029164442 -0.359319531274545 -
0.391259045165614 -0.314276962709309 -0.186924696051019 0
0.144932089263087 0.209544155068958 0.230906977474789
0.217974092341847 0.190262637051931 0.178547118636968
0.184568502403318 0.226325489826479 0.274889258898558
0.307378551307426 0.332616003267255 0.362683652204874
0.392070622977601 0.419297749573267 0.393680688636863
0.312012398814573 0.158440932843245 -0.0137182830155087 -
0.197134868524394 -0.531583466850974 -0.923104311310777 -
1.04261568910810 -0.955043825201847 -0.767634800456578 -
0.578916779240363 -0.383287256657556 -0.261026986271245 -
0.182055229179102 -0.114039772548773 -0.0544542531913333 -
0.0155508780748327 0.0114144492266449 0.0318871540322327
0.0361283025980963 0.00416260877760689 -0.0823358780224731 -
0.209072916339418 -0.290597216549904 -0.232464683275214 -
0.0992742923565079 -0.0262584692071667];
fourbar_spless_power=[-0.131636936773847 -0.326761090557930 -
0.347260832956349 -0.281810261168604 -0.305672715296254 -
0.366397741662386 -0.399851460229149 -0.321066283289484 -
0.190468376341428 0 0.146616135320101 0.211432240735535
0.232518882086933 0.219062054689547 0.190852077663254
0.178831262689955 0.184663377742550 0.226258953694611
0.274630378040390 0.306927029430986 0.331993759881842
0.361889188704382 0.391119397901151 0.418227204855232
0.392725669624643 0.311366256770540 0.158241856945931 -
0.0137203322776085 -0.197556119958269 -0.533747562157697 -
0.927571807653431 -1.04641110873631 -0.955310002248184 -
0.763781232478942 -0.572117067557001 -0.376024264508277 -
0.254331614258013 -0.176305999702437 -0.109922788907368 -
0.0522660047003091 -0.0148468627154992 0.0108303222729972
0.0301691793694556 0.0347530628698994 0.00415114576588607 -
0.0848985960989676 -0.218365149512696 -0.302004178370793 -
0.238339687005845 -0.100482672065309 -0.0264184365553872];
fourbar_sp_power=[-0.131636936773847 -0.323141761275832 -
0.338351835467859 -0.266547137419928 -0.277655599991857 -
0.309343790965155 -0.290065740836910 -0.135807349271216
0.0800436397967458 -0.345756752210243 -0.256283324562986 -
0.257569298979388 -0.320905256589922 -0.406196291129951 -
0.460984467638794 -0.462184575397225 -0.440032122240405 -
0.400038361397199 -0.346735346657056 -0.308833185094972 -
0.267414716963605 -0.221656132549837 -0.172146088347912 -
0.114422980132155 -0.0732016490491597 -0.0626643397039486 -
0.0599268194515229 0.0119487462162660 0.180590409655864
0.256905465694223 0.221056756056227 0.309369067703169
0.428826146006841 0.474989793756152 0.414126787997414
0.316352002225359 0.177042030521509 0.0633483334781121
0.00346290094994230 -0.0131646004454379 -0.0180556326716294
0.0373826082273507 0.0647379960530725 0.0583187827171553
0.00576350195271284 -0.102464741550905 -0.240450793232613 -
```

```
0.314573156953247 -0.240521632732260 -0.0994518131249730 -
0.0252571477573620];

plot(hip_power)
hold on
plot(fourbar_spless_power,'o')
hold on
plot(fourbar_sp_power)
grid on
ylabel('Power [W/kg]')
legend('Direct Drive','Fourbar','FourBar with Spring')
```